



HAL
open science

Optic flow cues help explain altitude control over sea in freely flying gulls

Julien Serres, Thomas J Evans, Susanne Akesson, Olivier Duriez, Judy Shamoun-Baranes, Franck Ruffier, Anders Hedenström

► **To cite this version:**

Julien Serres, Thomas J Evans, Susanne Akesson, Olivier Duriez, Judy Shamoun-Baranes, et al.. Optic flow cues help explain altitude control over sea in freely flying gulls. *Journal of the Royal Society Interface*, 2019, 16 (159), pp.20190486. 10.1098/rsif.2019.0486 . hal-02309725v2

HAL Id: hal-02309725

<https://amu.hal.science/hal-02309725v2>

Submitted on 16 Oct 2019

HAL is a multi-disciplinary open access archive for the deposit and dissemination of scientific research documents, whether they are published or not. The documents may come from teaching and research institutions in France or abroad, or from public or private research centers.

L'archive ouverte pluridisciplinaire **HAL**, est destinée au dépôt et à la diffusion de documents scientifiques de niveau recherche, publiés ou non, émanant des établissements d'enseignement et de recherche français ou étrangers, des laboratoires publics ou privés.

Optic flow cues help explain altitude control over sea in freely flying gulls

Research

Subject Areas:

computational biology, biomechanics

Keywords:

energy invariant, flight modelling, motion vision, optical invariant, visual neuroscience

Author for correspondence:

Julien R. Serres

e-mail: julien.serres@univ-amu.fr

Julien R. Serres¹, Thomas J. Evans^{2,5},
Susanne Åkesson², Olivier Duriez³, Judy
Shamoun-Baranes⁴, Franck Ruffier¹ and
Anders Hedenström²

¹Aix Marseille Univ, CNRS, ISM, Marseille, France

²Dept of Biology, CAnMove, Lund University, Ecology Building, SE-223 62 Lund, Sweden

³CEFE UMR 5175, CNRS - Université de Montpellier - Université Paul-Valéry Montpellier - EPHE – 1919 route de Mende, 34293 Montpellier cedex 5, France

⁴Computational Geo-Ecology, Inst. of Biodiversity and Ecosystem Dynamics, University of Amsterdam, P.O. Box 94 248, 1090 GE Amsterdam, The Netherlands

⁵Marine Scotland Science, Marine Laboratory, 375 Victoria Road, Aberdeen, AB11 9DB, Scotland, UK

Abstract

For studies of how birds control their altitude, seabirds are of particular interest because they forage offshore where the visual environment can be simply modeled by a flat world textured by waves then generating only ventral visual cues. This study suggests that optic flow, i.e., the rate at which the sea moves across the eye's retina, can explain gull's altitude control over seas. In particular, a new flight model that includes both energy and optical invariants help explain the gulls' trajectories during offshore takeoff and cruising flight. A linear mixed model applied to 352 flights from 16 individual lesser black backed gulls (*Larus fuscus*) revealed a statistically significant optic flow set-point of ca. $25^\circ/s$. Thereafter, an optic flow-based flight model was applied to 18 offshore takeoff flights from 9 individual gulls. By introducing an upper limit in climb rate on the elevation dynamics, coupled with an optic flow set-point, the predicted altitude gives an optimized fit factor value of 63% on average (30% - 83% in range) with respect to the GPS data. We conclude that the optic flow regulation principle helps gulls to adjust their altitude over sea without having to directly measure their current altitude.

1. Introduction

Understanding how a bird decides to fly at a given altitude during a specific manoeuvre is a difficult task because it is strongly dependent on the atmospheric conditions and flight capacity of the bird (see review [65]). Seabirds such as albatrosses and petrels flying close to the sea surface take advantage of the logarithmic increase in wind speeds to support dynamic soaring [55, 58, 59, 72], which works only at very low altitudes from ca. 0-10 m (see e.g. Fig. 5 in [62]). Birds flying by flapping flight at low altitudes over the sea could also use this windspeed gradient to reduce their transport costs. Under tailwinds, birds should fly higher where wind speed is high, while under headwinds birds should fly lower where wind speed is low. In terms of energy, a bird minimizing its transport cost should adjust its airspeed with respect to wind by increasing it in headwinds and decreasing it in tailwinds [27, 53]. This prediction comes from a U-shaped function between power required to fly and airspeed, which defines characteristic speeds for achieving minimum power V_{mp} and maximum range V_{mr} . During migratory [41] and homing flights [35] birds utilize wind assistance to minimize the transport cost and adjust airspeed accordingly to fly at the wind dependent V_{mr} .

Groundspeed is the combined effect of airspeed and wind speed (actually the airspeed and wind vectors). Wind assistance alone cannot be used by the bird to select a given groundspeed and a flight altitude. The altitude could be set by surrounding visual information seen by the bird. A bird can access information about its own motion with respect to its surrounding environment via the optic flow field through its early visual processing [4], as flying insects do in similar situations [4, 64]. The optic flow field perceived by an agent (a flying insect, a bird, or a human) is particularly dependent on the structure of the environment [20, 38, 49, 73]. Optic flow can be defined by a vector field of the apparent angular velocities of objects, surfaces, and edges in a visual scene caused by the relative motion between the agent and the scene (Fig. 1). The translational optic flow component is particularly interesting for birds positioning in space because it depends on (i) the ratio between the relative linear groundspeed of an object in the scene with respect to the bird, and (ii) the distance from obstacles in the surrounding environment. Consequently, optic flow requires neither groundspeed nor distance measurement, which is particularly useful to explain how birds perceive the world because birds are likely unable to sense directly their own groundspeed nor the 3D structure of the environment in which the binocular vision plays a minor role [42]. In addition, using depth perception based on motion parallax firstly requires a background and a foreground, then a head motion in translation. However, it has been reported for long-necked birds (whooper swans [57] and herons [34]) that exhibit a stabilization of their head, which could be the same for short-necked birds (like seabirds) while flying over sea, where seabirds perceive only a background. Consequently, motion parallax should play a minor role in altitude perception.

During flight manoeuvres, various optic flow parameters (such as the magnitude, the direction, the focus of expansion, the time-to-contact of optic flow) can be collected by birds to control their lateral position in straight tunnels (in budgerigars [7]), to decrease their speed in a converging tunnel (in budgerigars [63]), to plunge into water (in gannets [39]), to hover (in hummingbirds [21, 60]), and finally to land (in hawks [12] and in hummingbirds [40]).

In this study, we address the question of how seabirds control their altitude during offshore takeoffs and cruise flights with respect to wind. Here, two working hypotheses were compared about altitude control:

- a first hypothesis based on a direct measurement and regulation of optic flow that adjusts the altitude, and,
- a second hypothesis based on a direct measurement of the barometric pressure that directly regulates the altitude itself.

To test these alternative hypotheses, a statistical analysis of 352 flights comprising 16 individual lesser black-backed gulls (*Larus fuscus*) in various wind conditions were conducted.

Then, 18 offshore takeoffs followed by a cruise flight were analyzed by taking into account morphological parameters from 9 individual gulls.

2. Modelling the flight in terms of groundspeed and altitude: a theoretical approach

(a) How is bird groundspeed deduced from aerodynamic effects?

The relationship between:

- the bird's ground speed V_g
- the bird's airspeed V_{air}
- the wind speed V_w

is given by equation (2.1):

$$V_g = V_{air} + V_w \quad (2.1)$$

The basis for deriving predictions about bird flight is the so-called flight mechanical theory, which combines the relationship between power output P and airspeed V_{air} in flapping flight as follows:

$$P(V_{air}) = a + b \cdot V_{air}^{-1} + c \cdot V_{air}^3 \quad (2.2)$$

where a , b , and c represent various physical, morphological and physiological properties of the bird and air [52, 54, 56]. If the objective is to minimize the energy cost per unit distance (i.e., cost of transport), the optimal flight speed is the maximum range speed V_{mr} [27, 52]. The maximum range speed V_{mr} is obtained from the U-shaped power curve [25, 28, 56] by the condition:

$$\left(\frac{\partial P}{\partial V_{air}} \right)_{V_{air}=V_{mr}} = \frac{P(V_{mr})}{V_{mr}} \quad (2.3)$$

Indeed, a gull's homing flight is similar to a migratory flight, in that it is assumed that the flight's objective is principally for transportation, as opposed to outbound foraging flights when the bird is likely also searching for food. Seabirds' homing flight over the sea is therefore a directed flight between two locations. During transport flight gulls are expected to minimise overall energy expenditure or time, thus cost of travel per unit distance should be minimised rather than instantaneous energy expenditure. If minimising the cost of travel per unit distance birds will travel at maximum range speed (V_{mr}) not minimum power airspeed (V_{mp}). V_{mr} refers to V_{air} rather than V_g . If a bird experiences a tailwind, its cost of travel per unit distance decreases, thus V_{mr} also declines. Conversely under headwinds V_{mr} increases. In a recent work, it was analyzed how lesser black-backed gulls (and guillemots) modulate their airspeeds in relation to winds [18]. It was found that gulls increased airspeeds under headwinds and decreased airspeeds under tailwinds [18], and similar behaviour has been observed during longer distance homing flights [46]. These results suggest that gulls are flying at V_{mr} rather than V_{mp} , since V_{mp} should not be affected by winds like V_{mr} [18].

(b) Optic flow vector field generated by a bird in flight over sea

Consider a bird flying over the sea at an altitude h and a groundspeed V_g (neglecting vertical speed V_z) the magnitude of the ventral optic flow field ω can be expressed as follows:

$$\omega(\phi, \theta) = \frac{V_g}{h} \sin^2 \theta \times \cos \phi \quad (2.4)$$

with θ the elevation angle and ϕ the azimuth angle.

The magnitude of the ventral optic flow field is plotted in Fig. 1a with the projection of its elevation and azimuth angles over the sea. The larger projection of vector magnitude of optic

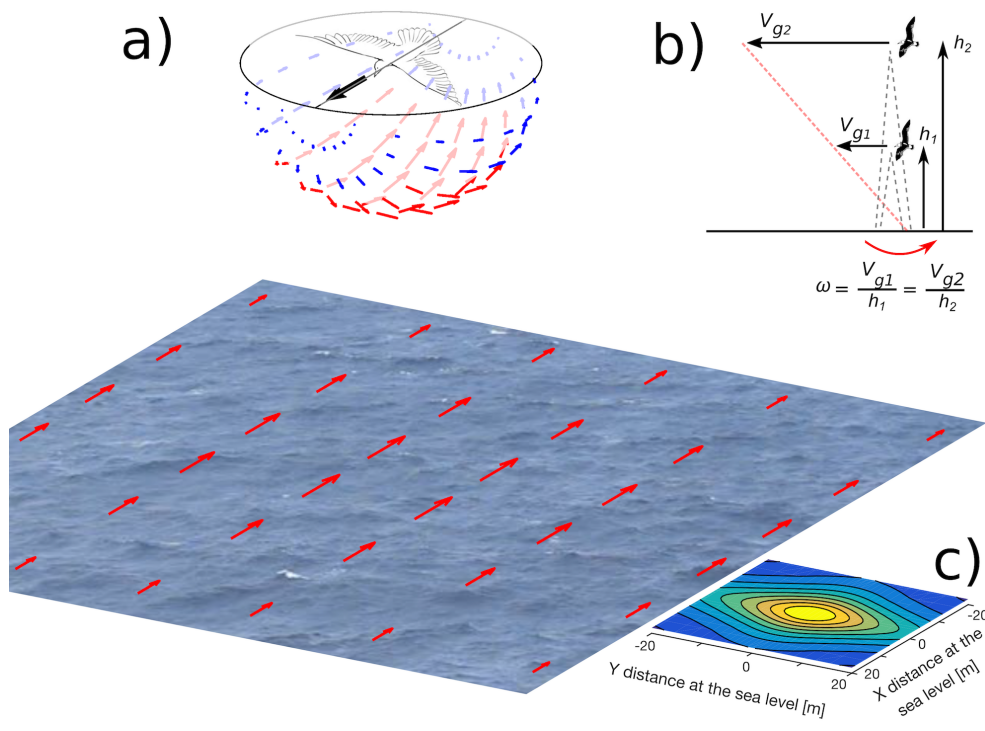


Figure 1. (a) A gull flying over the sea generates a vector field of optic flow. Such a vector field is perceived by a gull based on the contrasts created by waves and white-crested waves (also called white-horses). Inspired by [20]. (b) The magnitude of the vector of the optic flow, ω , is determined by the gull's groundspeed, V_g , and its altitude, h . If ω is held constant by adjusting the altitude, h will always tend (through the bird dynamics) to be proportional to V_g (only a linear combination -red dashed line- between h and V_g is asymptotically possible). (c) Optic flow magnitude in the ventral field of view at 10m-height where the magnitude of the ventral optic flow $\omega(\phi, \theta) = \frac{V_g}{h} \sin^2 \theta \times \cos \phi$ is projected at the sea level with ϕ the azimuthal angle and θ the elevation angle. (The magnitude of vertical optic flow is the maximum and is $\omega(\phi = 0^\circ, \theta = -90^\circ) = \frac{V_g}{h}$)

flow over the sea is shown using a contour plot in Fig. 1c in the case of a bird flying at a height of 10 m. The bird may be able to perceive the optic flow maximum from a non-negligible area of its field of view (Fig. 1c). The maximum magnitude of the ventral optic flow is always vertically downwards from the bird in the direction of the sea :

$$\omega(\phi = 0^\circ, \theta = -90^\circ) = \frac{V_g}{h} \tag{2.5}$$

(c) How the model predicts the bird's flight height from the ventral optic flow regulation principle

The ventral optic flow regulation principle tends to keep constant the vertically downward optic flow whatever the speed or height of flight by adjusting the altitude [19, 61]. Here, it introduces this asymptotic proportionality relationship for birds: the bird's height of flight h will always tend (through the bird dynamics) to be proportional to the bird's ground speed V_g (Fig. 1b) as :

$$\omega_{sp} = \omega(\phi = 0^\circ, \theta = -90^\circ) = \frac{V_g}{h} = \text{constant} \tag{2.6}$$

where ω_{sp} is the ventral optic flow set-point. Besides, the wind profile power-law is often used to estimate the horizontal wind speed [32] as follows:

$$V_w = V_{ref} \cdot \left(\frac{h}{h_{ref}} \right)^\alpha \quad (2.7)$$

with the parameter α is the power-law exponent (that is usually specified as a function of stability as well as the roughness of the surface $0 < \alpha < 1$ (here over seas $\alpha = 0.11$ see [31]), the speed V_{ref} as being the wind speed at a reference height h_{ref} (10m). By combining (2.6) and (2.7) into (2.1), we obtain:

$$\omega_{sp} \cdot h = V_{air} + V_{ref} \cdot \left(\frac{h}{h_{ref}} \right)^\alpha \quad (2.8)$$

To find the bird's steady-state flight height h reached during a takeoff as function of the wind profile, it requires to solve the equation $f(h) = 0$ with the function f defined as follows:

$$f(h) = V_{air} + V_{ref} \cdot \left(\frac{h}{h_{ref}} \right)^\alpha - \omega_{sp} \cdot h \quad (2.9)$$

In the variation table of the function f (Tab. S1), we observe that only one unique altitude h exists, enabling $f(h) = 0$ during an offshore takeoff manoeuvre. We can therefore conclude that both the minimisation of the rate of energy consumption and regulating the ventral optic flow enable a bird to fix both its groundspeed and its altitude above the sea. The bird's steady-state flight height h cannot be considered as a "target flight height" or a "desired flight height", but as an "optimal flight height" because the bird's altitude is adjusted as a function of the wind conditions (higher under tailwinds but lower under headwinds) and thereby maximizing positive effects as well as minimizing adverse effects of the wind gradient.

3. Materials and Methods

(a) Ethics statement

Permissions to capture and ring birds were from granted the Swedish Nature Protection Board (Naturvårdsverket) and the Swedish Ringing Office at the Natural History Museum in Stockholm. Ethical permission to tag the gulls was from granted Malmö/Lund Djurförsöksetiska nämnd (No. M112-09, M470-12). Permission to work in the protected area was from the county administration Länsstyrelsen Gotlands Län.

(b) Gulls' trajectory recording

16 lesser black-backed gulls (*Larus fuscus*) were GPS tracked from their breeding colony on Stora Karlsö island, Sweden (17.972° E, 57.285° N) during May to September of 2013-2015. The island is a small offshore island (2.5 km²) located in the western central Baltic Sea, sited 7 km west of the much larger island of Gotland (Fig. 2a). During breeding the gulls perform central-place foraging trips [51], flying out from their island to forage, either at sea or on land [33].

Gulls were caught during late incubation (late May) using walk-in traps set over their nests. They were weighed and sexed from morphological measurements [11] or genetically [24] from a few breast feathers taken at capture. The GPS devices are ca. 18 g (size: 61×25×10 mm), are solar-powered, have 4 MB of memory for data storage, include a tri-axial accelerometer, and have a short-range communication system. They were developed at Amsterdam University (<http://www.uva-bits.nl/gps-trackers/>), and we used the UvA-BiTS model 4CDLe during the study (see [9] for GPS device detail). The GPS device was mounted using either a full body or wing harnesses [70] constructed of tubular TeflonTM ribbon (Bally Ribbon Mills 8476-.25") (full tagging procedure given in [33], see Fig. 3). Data were downloaded and programs uploaded to the GPS devices remotely using a network of four antennas providing good coverage of the colony area. GPS tracking was continuous though the location intervals varied depending on the requirements of parallel studies (e.g. [33]). At a 6 seconds interval on a white stork (*Ciconia ciconia*)

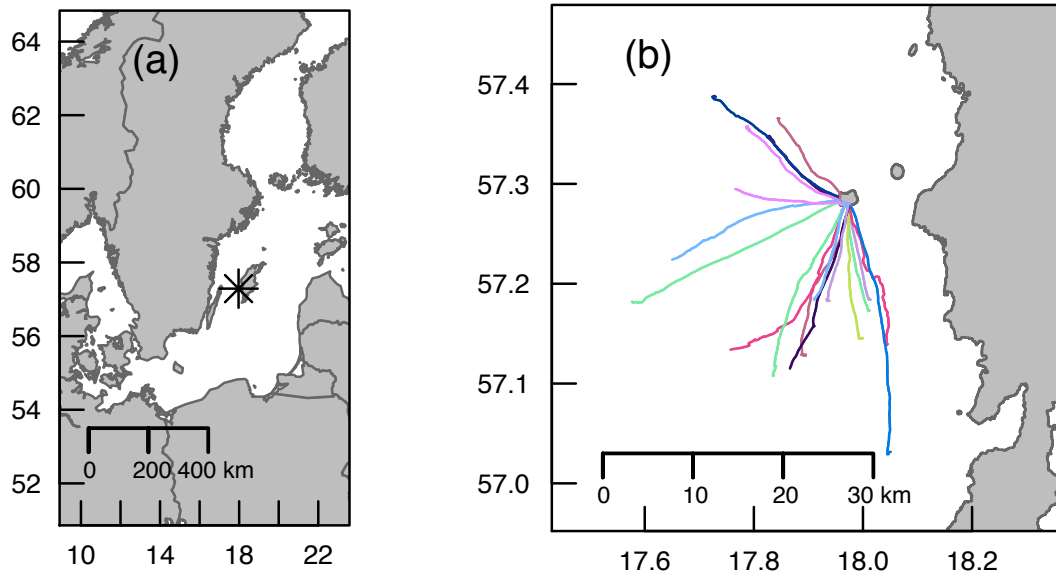


Figure 2. (a) Study location of the island of Stora Karlsö (indicated by *asterisk), Baltic Sea, Sweden. (b) From this site Lesser Black-backed Gull (*Larus fuscus*) inbound flights were tracked with GPS (18 flights from 9 individual gulls, coloured lines).

on its nest, it was quantified a mean altitude error of 2.77 m and a mean speed error of 0.02 m/s of the UvA-BiTS device [9].



Figure 3. Lesser black-backed gull (*Larus fuscus*) equipped with an 18 g solar-powered UvA-BiTS device (size: 61×25×10 mm). The GPS unit used is the Lea-4S chip from U-blox manufacturer. See [9] for UvA-BiTS detail. Photographic credit: the authors.

The continuous GPS tracks were segmented into foraging trips and within these, sections of continuous flight, with the final flight of a foraging trip considered a homing flight, as the gulls returned from presumed foraging at sea (only marine trips were used in this study, c.f. [33]) to the island colony. 18 takeoffs from 9 individual gulls with high resolution data were selected (i.e. 10 or 15-second intervals), and we selected only takeoffs reaching a steady-state altitude - i.e. not those with a constantly fluctuating altitude. In addition, the final altitude had to be greater than 10 m with variation in altitude during the ascent until reaching a steady-state altitude. No information

about the presence or absence of boats in the area around the island of Stora Karlsö was known, likewise if birds flew alone or with other birds.

Flight GPS points were annotated with wind data extracted from a global weather model, ERA-interim data [14] provided by the European Centre for Midrange Weather Forecasts (ECMWF, <http://www.ecmwf.int/en/research/climate-reanalysis/era-interim>), which gives variables at 3-hour intervals and is gridded with a spatial resolution of approximately 79 km. These were extracted using the environmental-data automated track annotation (Env-DATA) system [15] hosted by MoveBank (<http://www.movebank.org/>).

(c) Takeoff time series analysis: individually tuned parametric model

Parametric model estimation

The linear parametric models about each gull's elevation dynamics were estimated with the System Identification Toolbox from the Matlab software (parameters : time constant τ_h and static gain $\frac{1}{\omega_{sp}}$ in (3.2). The maximum climbing speed V_{zmax} (3.1) was computed from [25, 53]:

$$V_{zmax} = \frac{2.16 \cdot m_m \cdot f}{m} - \frac{1.92 \cdot m^{\frac{2}{3}}}{\rho^{\frac{1}{2}} \cdot b^{\frac{3}{2}}} \quad (3.1)$$

where m_m is the mass of the flight muscles, f is the observed flapping frequency (3.26 Hz on average, see page 162 in [18]), m is the total mass including any added load, ρ is the air density (1.205 kg/m³ at 20°C) and b is the wing span. The vertical wind is low over the sea, consequently in flight, we neglected the vertical wind. For each of the 18 offshore takeoffs followed by a cruise flight, we took into account the morphological parameters of each gull.

Computation of the predicted altitude

The model output, i.e. the predicted altitude, h_{est} , was computed with the Simulink environment from the Matlab software. The best fit factor of the optic flow-based control model is obtained by adjusting the flight muscle fraction ($\frac{m_m}{m}$) instead of the bird mass m , because the bird mass was known without any prey load. The fit factor considered was the goodness of fit between optimized simulated data (h_{est}) and actual GPS data (h_{GPS}) using a Matlab function with a normalized mean square error cost function (called NRMSE cost function). NRMSE fit factor varies between minus infinity (worse fit) to 1 (perfect fit). According to the table 15 in [22], the flight muscle ratio ($\frac{m_m}{m}$) is relatively constant across birds species at 0.18 ± 0.05 (MEAN \pm SD, with $n = 221$). Our simulated model has been adjusted with the flight muscle ratio in order to get the best fit factor, then adjusting the maximum climbing speed in the elevation dynamics model. For our group of 9 individual lesser black-backed gulls, we obtained the best fit factor with a corresponding distribution of flight muscle ratio ($\frac{m_m}{m}$) of 0.18 ± 0.03 , which is quite similar to prediction 9 from [25]. The optic flow-based control model takes into account the observed correlation between the groundspeed V_g and the altitude h coming from gulls' GPS data. The proportionality factor is called here a ventral optic-flow set-point ω_{sp} (2.6). Once the best fit factor has been reached by adjusting the flight muscle fraction $\frac{m_m}{m}$, each gull's altitude is re-computed by considering an altitude control model that directly feeds the elevation dynamics with a "target flight altitude", noted an altitude set-point h_{sp} , which is computed when the gull reached its steady-state altitude.

Optic flow-based altitude control model

We consider two scales of time. The gull's forward dynamics (Fig. 4a) responds faster than the gull's upward dynamics (constrained by V_{zmax} see (3.1), see Fig. 4b) because the height of flight arises from the response of a first order differential equation by considering the forward speed as

a step input (3.2). The bird's elevation dynamics is represented in Fig. 5a, this includes both the first order upward dynamics (3.2) and the maximum climbing speed V_{zmax} (3.1).

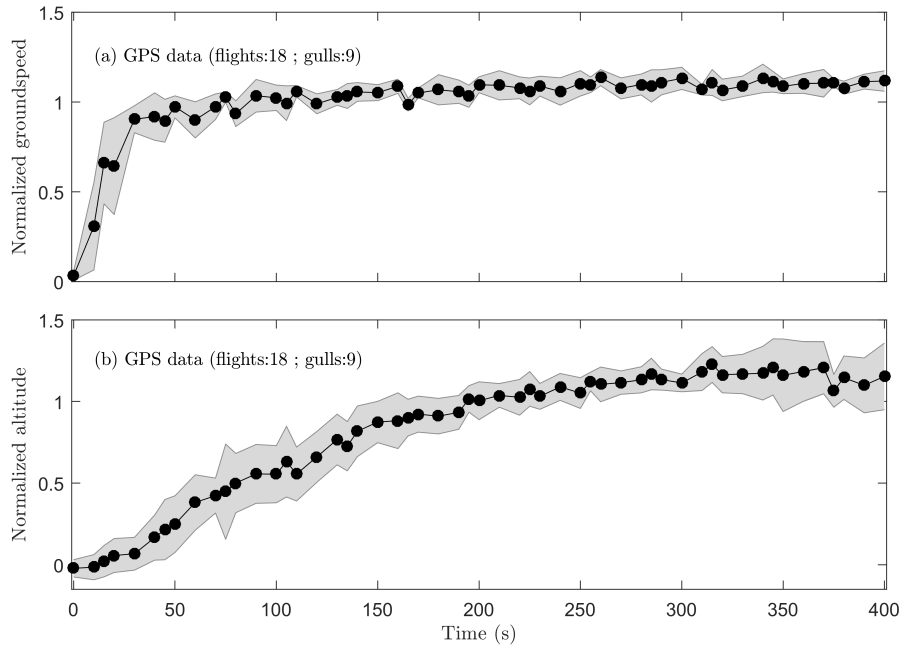


Figure 4. The gull's forward dynamics (in (a)) versus the gull's upward dynamics during offshore takeoffs (in (b)). (a) Normalized groundspeed coming from GPS speed measurements $\frac{V_{gGPS}}{\text{mean}(V_{gGPS})}$, which is computed by the current groundspeed to average groundspeed ratio. (b) Normalized altitude coming from GPS data, which is computed by the current altitude to average altitude (by removing the first 100 seconds) ratio $\frac{h_{GPS}}{\text{mean}(h_{GPS}(100s:end))}$. Black dots represent GPS data recorded at a sampling time 10 s (12 trajectories) or 15 s (6 trajectories). Each dot represents the median value and shaded areas represent the median absolute deviation (MAD) of the GPS data collected from 18 flights.

$$\tau_h \cdot \frac{dh}{dt} + h(t) = \frac{1}{\omega_{sp}} \cdot V_g(t) \quad (3.2)$$

An explicit solution of equation (3.2) can be written, if we consider a step response at a given positive amplitude V_{g0} value, as follows:

$$h(t) = \frac{V_{g0}}{\omega_{sp}} \cdot \left(1 - e^{-\frac{t}{\tau_h}}\right) \quad (3.3)$$

For each gull trajectory, we consider only one takeoff followed by a cruise flight, and then we perform a first order system identification described by the differential equation (3.2). In this model, a proportionality factor $\frac{1}{\omega_{sp}}$ is introduced, which is the inverse of the ventral optic flow set-point ω_{sp} (2.6), and the input of the upward dynamics (3.2) is the groundspeed V_g , which correlates the altitude h and the groundspeed V_g . If the gull's groundspeed is constant during takeoff as well as during cruising flight, then the predicted altitude profile will be the same with both models.

The inter-flight variability of the climb time constant ($\tau_h = 97.3s \pm 68.0s$, with $n = 18$ takeoffs in Fig. 4b) was derived on the basis of morphological properties of the birds (*inter alia* age, wingspan, body mass including the load of prey and sex).

Direct altitude control model

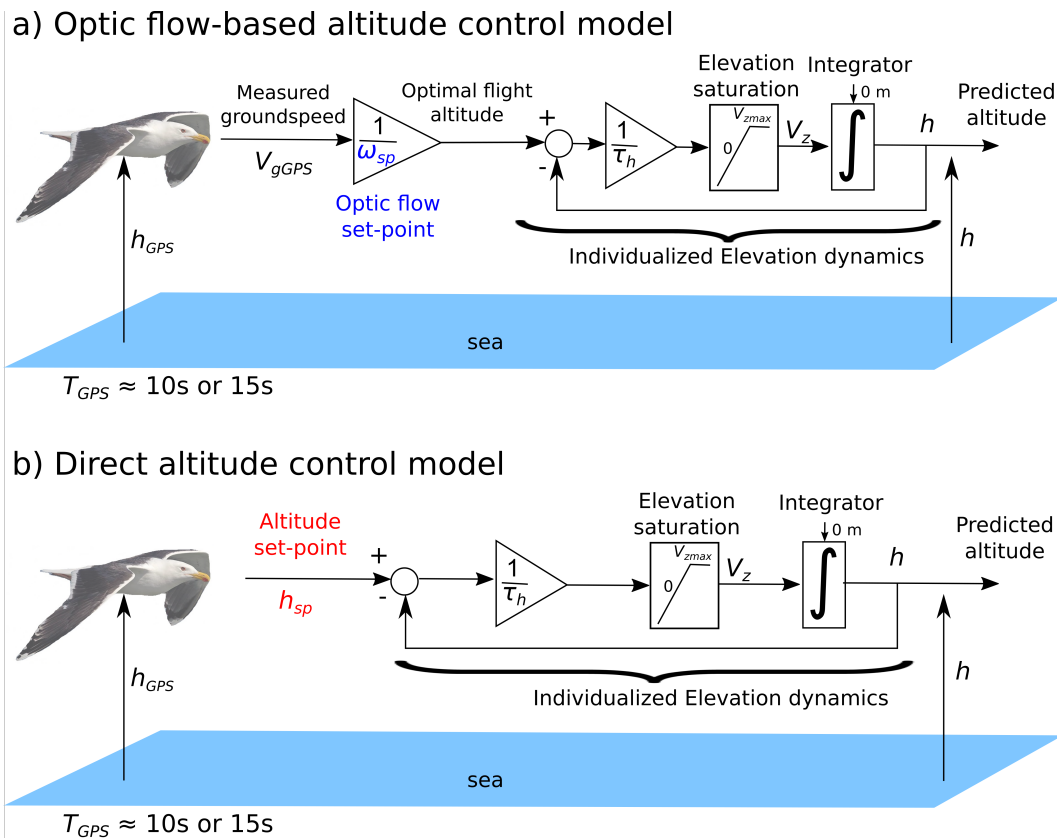


Figure 5. (a) Optic flow-based altitude control model including an individualized gull's elevation dynamics. Once the gull has reached the minimum groundspeed to takeoff, groundspeed is then relatively constant during its flight, an optic-flow-based control system can be switched on and lead the gull to a given altitude depending on both its groundspeed V_g and its ventral optic flow set-point ω_{sp} . The ventral optic-flow set-point ω_{sp} is an internal parameter used by the gull to tend asymptotically to its optimal flight altitude proportionally to its current groundspeed V_g . This model correlates the gull's current groundspeed to its current altitude. (b) Direct altitude control model. Here, the model only includes an individualized elevation dynamics and an altitude set-point h_{sp} . This model does not impose asymptotically any proportionality between groundspeed and altitude. The altitude set-point h_{sp} is an internal parameter used by the gull to select its "desired" or "target" flight altitude.

Here, the bird's elevation dynamics is represented in Fig. 5b, which includes both the first order upward dynamics (3.4) and the maximum climbing speed V_{zmax} (3.1).

$$\tau_h \cdot \frac{dh}{dt} + h(t) = h_{sp} \quad (3.4)$$

An explicit solution of equation (3.4) can be written, if we consider a step response at a given altitude h_{sp} value, as follows:

$$h(t) = h_{sp} \cdot \left(1 - e^{-\frac{t}{\tau_h}}\right) \quad (3.5)$$

The "target flight altitude", also called the altitude set-point is denoted h_{sp} , which is computed from when the gull reached its steady-state altitude, i.e. the gull's mean altitude when $t > 3\tau_h$ or $t > 5\tau_h$, depending on data availability. In this model, there is no correlation between altitude and groundspeed.

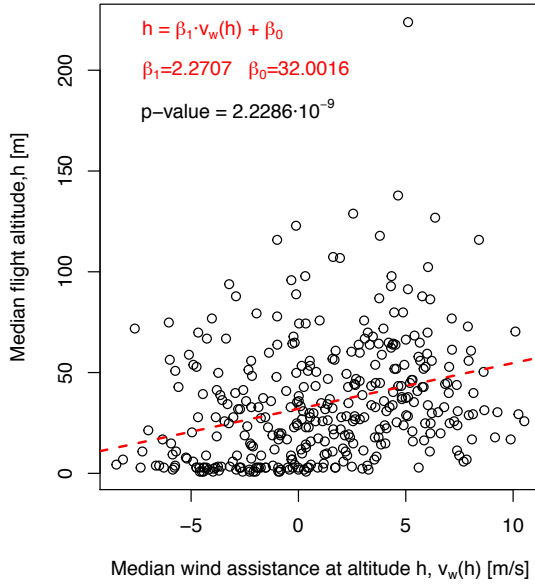


Figure 6. Gull's median altitude h versus median wind assistance V_w (head or tail wind) at median altitude h for 352 flights (16 distinct gulls). The regression line using β_1 and β_0 is plotted in red. See Table S2 for dataset details.

4. Results

(a) Full flights' dataset analysis: statistical model

The dataset here includes all inbound (returning to the island colony) over sea flights by the lesser black-backed gulls (383 flights, 16 gulls). The dataset is composed of median altitudes h calculated per flight, median wind speed measured at 10m-height (from ECMWF data), V_{ref} , and the gull identifier. After excluding the flights endowed with a median altitude below zero meters, the data comprise 352 observations of 16 individual gulls (see Table S2).

A nonlinearity of wind profile power law (2.7) was introduced to estimate the wind speed $V_w(h)$ experienced by gulls at their median altitude h calculated per flight. A linear mixed effect model was designed using *lmer* in R software for the ordinates (β_i is the constant random effect) as follows:

$$h = \beta_1 \cdot V_w(h) + \beta_0 + \beta_i + \varepsilon_{i,V_w} \quad (4.1)$$

with the regression parameters: $\beta_1 = 2.2707$ and $\beta_0 = 32.0016$. The Kenward-Roger corrected F-test was used to calculate the significance level of the linear mixed model (ndf:1, ddf: 347.89, Fstat: 37.722, p.value: $2.2286 \cdot 10^{-9}$, F.scaling: 1). The parameter β_1 was highly significant (Fig. 6). Using the coefficient $\beta_1 = 2.2707$, an identification of the ventral optic flow set-point $\omega_{sp-lmer}$ can be performed using the equation (2.8) that includes the wind profile power law as follows:

$$\omega_{sp-lmer} = \frac{1}{\beta_1} = 0.4403 \text{ rad/s} = 25.23^\circ/\text{s} \quad (4.2)$$

This statistical analysis tells us that gulls tend to maintain a ventral optic flow close to $25.23^\circ/\text{s}$ whatever the wind conditions are while flying above the sea.

(b) Comparison between optic flow-based and direct altitude control models

In this section, 18 takeoffs are treated as independent observations despite these being recorded on 9 individual birds. Indeed, the weather, the wind, the state of the sea, the moment, and the fishing area were uncontrolled and different from one flight to another (Fig. 2b).

A set of 18 trajectories representing 9 different gulls are individually shown in the horizontal plane in Fig. 2b. The set of GPS data are clustered and shown in Fig. 4 for the initial 400 seconds of each flight. It allows us not only to show the increase in speed during the gulls takeoff (Fig. 4a), but also their level flight along the vertical plane (Fig. 4b). Both groundspeed and altitude have been individually normalized by the steady state value reached by the gull's groundspeed and altitude, respectively (Fig. 4). Consequently, both curves reach a steady state close to a value of one (Fig. 4).

A linear 1st order parametric model on the data (18 trajectories) gives a fit factor value (i.e., a normalized mean square error cost function, called NRMSE cost function) of 40.4% on average (range: 10-80%). Then, by introducing a constraint on the climb rate according to prediction 10 in [25, 53], a direct altitude control model based on a non-linear 1st order parametric model combined with an altitude set-point h_{sp} (see Fig. 5b for details) gives a fit factor of on average 57.1% (range: 11-77%). However, by adding to the previous model a correlation between groundspeed and altitude, which is linked to what we call an optic flow set-point ω_{sp} (see Fig. 5a for details), an optic flow-based control model gives a fit factor of 63.4% on average (range: 30-83%).

Examples comparing an optic flow-based control model to a direct altitude control model for one takeoff is given in Fig. 7b (the 17 other takeoffs are shown in Supplemental Information, Figs. S4-S20). We observe that in each case the fit factor was higher with an optic flow-based control model (blue dots in Fig. 7b rather than a direct altitude control model (red dots in Fig. 7b).

The set of normalized predicted altitudes ($n = 18$) computed with an altitude control model (Fig. 5b) is shown in Fig. 8a, and with an optic flow-based control model (Fig. 5b) is shown in Fig. 8b. Residuals, which are the errors between altitudes coming from GPS data and predicted altitudes coming from models, are represented in Figs. 8c-d. We compared the residuals distribution between the two models in transient response (white shaded boxes in Fig. S3) and in steady-state response (gray shaded boxes in Fig. S3). The median value of the residuals (Figs. 8c-d) coming from the optic flow-based model was significantly higher in transient response (one-sided Wilcoxon rank sum test, $n = 27$, $p \ll 0.001$) and was also significantly higher in steady-state response (one-sided Wilcoxon rank sum test, $n = 27$, $p \ll 0.001$). Consequently for both parts, the response predicted by the optic flow-based control model was better than the response predicted by the altitude control model. Finally, the average value of the residuals coming from each control model in transient response, then in steady-state response, were compared to a normal distribution centred around zero. The distributions of residuals with the optic flow-based control model (white shaded boxes in Fig. S3) were not significantly different from a normal distribution centred around zero (t -test, $n = 27$, $p = 0.95$ in transient response, and $p = 0.07$ in steady-state response). Residuals with the direct altitude control model (gray shaded boxes in Fig. S3) were significantly different from a normal distribution centred around zero (t -test, $n = 27$, $p < 0.01$ in transient response and $p \ll 0.001$ in steady-state response). This statistical analysis shows that the optic flow-based control model is the most established model. Besides, for 13 out of 18 flights, we observe a significant correlation (Spearman's test on GPS data) between groundspeed and altitude (ρ from 0.22 to 0.83, 13 flights). We therefore conclude that our optic flow-based control model (Fig. 5a) better explains the gulls' GPS tracking data than the direct altitude control model (Fig. 5b).

5. Discussion

(a) Comparison of optic flow set-points identified by both analyses

We compared the distribution of ventral optic flow set-points coming from the tuned parametric model obtained from the takeoff time series ($\omega_{sp} = 22^\circ/s \pm 9^\circ/s$ with $n = 18$, Shapiro normality test: $p = 0.16$) and the parameter $\omega_{sp-lmer} = 25.23^\circ/s$ obtained from the linear mixed effect model (4.2), respectively. No significant difference was observed between the ω_{sp} distribution

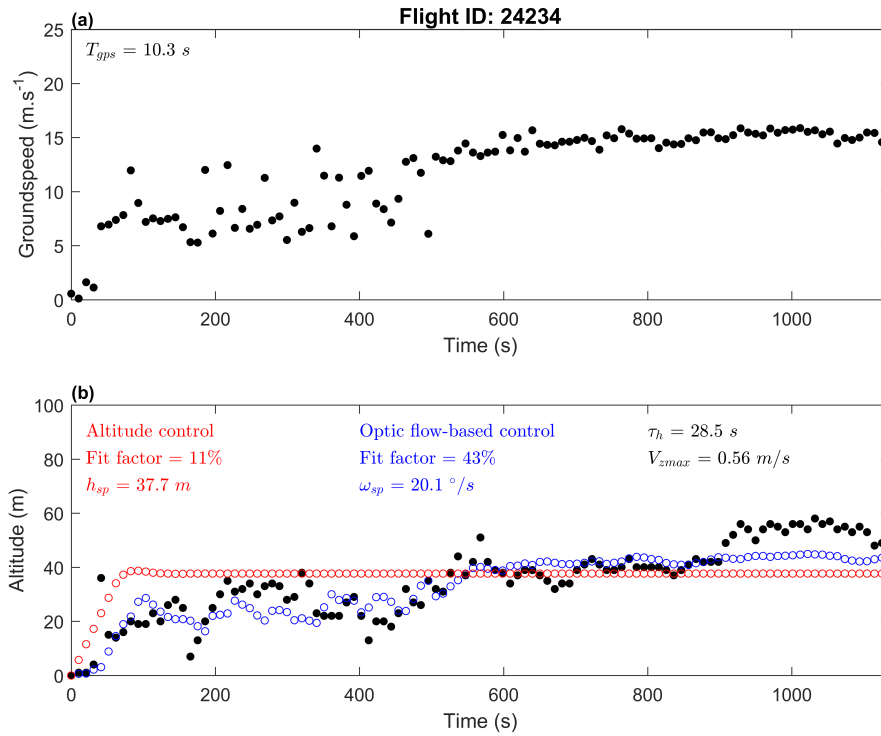


Figure 7. (a) Groundspeed of the gull ID24234 tracked with the GPS. (b) Altitude of the gull: black dots represent the GPS data, red dots represent the gull altitude on the basis of an altitude-based control model (fit factor: 11%), and the blue dots represent the gull altitude on the basis of an optic flow-based control model (fit factor: 43%). A significant correlation was observed between groundspeed and altitude of the GPS data ($\rho = 0.83$, $p \ll 0.001$ by Spearman's test).

and the value $\omega_{sp-imer}$ (t -test, $t:1.5296$, $df: 16$, p -value:0.1457). This suggests shows that both analyses identify optic-flow set-points that are in the same range and not significantly different. As a consequence, both the takeoff time-series and the full dataset support the ventral optic flow regulation hypothesis in a consistent manner.

(b) Effect of wind on the birds' altitude

An additional outcome of the ventral optic flow regulation hypothesis [19, 61] is that any increase in headwind will lead to a decrease in gull flight altitude in order to maintain the ventral optic flow constant (Fig. 10a). Conversely, any increase in tailwind will lead to an increase in bird altitude (Fig. 10c). A bird can adjust its ground speed by adjusting its airspeed or its heading relative to ground (and wind), thus allowing it to minimize its cost of transport in flight. The altitude control system based on optic flow is therefore consistent with previous observations on speed adjustment with respect to winds in migrating birds [2].

The small Hellman exponent α over relatively smooth surfaces, such as the sea, means that wind speed increases more rapidly than over a rough surface (e.g. a forest). Thus at higher altitudes (i.e., from 10 m to 100 m) wind speed will not vary much, but below 10 m wind speed can double going from 1 m to 10 m. Around the sea's waves wind is deflected leading to a pattern of updrafts and downdrafts [55, 59, 74]. Together these effects are used by soaring seabirds in dynamic soaring, gust soaring or "sweeping flight" [55, 59, 74], and the characteristic meandering flight style that results has been termed "wave-meandering wing-sailing" [67]. Flapping seabirds can also use these features to gain a higher climb rate at the start of a take-off maneuver, taking

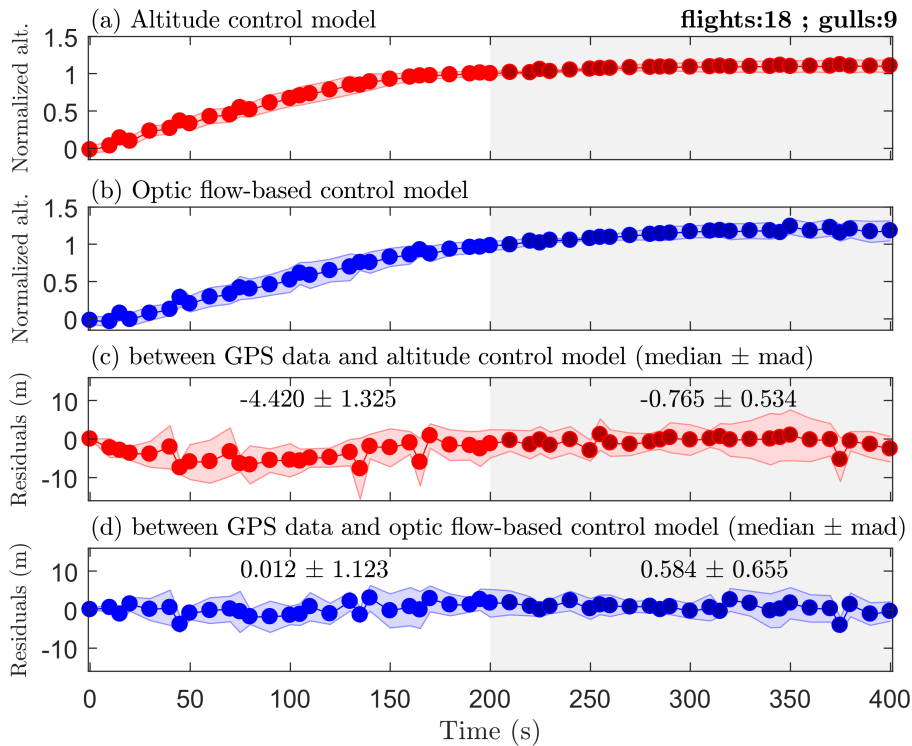


Figure 8. Red dots (altitude control model) or blue dots (optic flow-based control model) represent predicted altitude ((a) and (b)) or residuals ((c) and (d)) at a same sampling time 10 s (12 trajectories) or 15 s (6 trajectories) like GPS data (see Fig. 4). Each dot represents the median value and shaded areas represent the median absolute deviation (MAD) of data ($n = 18$). The white shaded areas represent the transient response (time < 200 s) during takeoff and ascent, and the gray shaded areas represent the steady state response (time > 200 s) once in cruising flight. The duration $200 \text{ s} \approx 2 \cdot \tau_h$ represents about 86% of the step response of a 1st order dynamic system (see (3.3)). (a) Normalized predicted altitude using an **altitude control model** (Fig. 5b), which is computed by current predicted altitude average predicted altitude (by removing the first 100 seconds) ratio $\frac{h}{\text{mean}(h(100s:end))}$. (b) Normalized predicted altitude using an **optic flow-based control model** (Fig. 5a), which is computed by current predicted altitude average predicted altitude (by removing the first 100 seconds) ratio $\frac{h}{\text{mean}(h(100s:end))}$. (c) Residuals between GPS data (Fig. 4b) and altitude computed with the altitude control model (data in (a)). (d) Residuals between GPS data (Fig. 4b) and altitude computed with the optic-flow based control model (data in (b)).

off facing into the wind in the updraft formed by the deflection of the wind over a wave (see page 268 in [56], and [35]), which therefore reduces the effort required to take-off and accelerate to reach the maximum range speed V_{mr} . Seabirds may also use the "ground effect" while flying very close to the sea to reduce their energetic expenditure [8], which is helpful for takeoff at sea.

(c) Effect of altitude on optic flow

According to prediction 3 in [25, 53], the optimal altitude for a migratory bird is that where it can get just sufficient oxygen to maintain its cruising airspeed. This arises from the power required to fly at maximum range speed decreasing with altitude due to decreasing air density. Consequently, at an altitude of 6000 m, where the air density is half that at sea level, a bird should theoretically fly $\sqrt{2}$ times faster. On the other hand, at a given optic-flow set-point working in a 100 m altitude range, the optic flow would be divided by a factor $\frac{60}{\sqrt{2}}$ at an altitude of 6000 m. Therefore the optic flow would be too small to be maintained at the amplitude of the one generated in a 100 m altitude

range. Recently, McLaren and colleagues (2016) analysing flights of lesser black-backed gulls flying between south-east England and The Netherlands recorded much greater flight altitudes than those observed here during homing flights to the breeding colony, with maximal values 1,240 m [46], even though typical values were lower at 100-150 m. On migratory flights, the gulls have been recorded flying higher still, though that is overland, with maximal altitudes around 5,000 m (unpublished data). Consequently, an optic flow based altitude control system can only work below a 100-meter altitude range where the optic flow is significant and detectable by the visual system of the birds.

(d) Are groundspeed and altitude still proportional at higher altitudes?

Birds making lower altitude flights (<100-150 m) will generate a detectable optic flow. However, when on long distance or migratory flights birds may fly higher at hundreds to thousands of meters (see above), optic flow values will then be extremely low, thus unlikely to be suitable for regulating a given optic flow set-point. This relates to the finding for common swifts (*Apus apus*) by Hedenström & Åkesson (2017), that the swifts did not compensate for head- and tail winds as expected from flight mechanical theory when flying at high altitudes (>1000 m), but they did so at low altitudes (<100 m) [26]. This was interpreted as a failure to detect small changes in optic flow due to winds by the swifts' visual system at high altitudes. In addition, for altitudes higher than 400 m, lesser black-backed gulls were observed to compensate less for cross-wind disturbance than they did at lower altitudes: fractional compensations were observed to decrease from about 1.3 (on average) to less than 0.5 at 900 m height [46]. At altitudes above 400 m, gulls' groundspeed may be highly dependent on the wind speed: no altitude increase or decrease can be predicted with respect to the optic flow-based control model as optic flow is low thus its changes with altitude would be difficult to detect by the gulls' visual system.

(e) Can birds use barometric pressure to determine altitude?

The birds' mechanoreceptive paratympanic organ (PTO) is located in the middle ear, and it is probably used by birds to detect barometric pressure [71]. Birds appear to use the PTO not only as a barometer to predict the onset of inclement weather [10, 66, 71], but also as a genuine altimeter to adjust their flight altitude during migration. Birds can fly level within $\pm 20\text{m}$ for distances of 2-3km at altitudes of 700 - 1,100m, even at night [23], i.e. without visual cues. However, it is still an open question whether birds can use changing barometric pressure directly to measure their current altitude in real time.

A mechanoreceptive scale sensory organ found in fish [5] may play the same sensory function as the PTO in birds. It is known that fish can determine their depth using hydrostatic pressure [30, 69]. On this point, it was demonstrated that the dynamic depth sensing in fish is less than 1 m at a depth of 100 m [69]. However, water density is approximately 1,000 times higher than air density, and the pressure gradient in flight is therefore particularly low generating extremely low frequencies in the feedback signal to the bird's elevation dynamics. Therefore, it would be difficult to adjust the flight altitude for a short period of time, only being practical for long periods of time such as for example during longer distance migratory flights.

A bird does not have to compute its altitude from other physical or internal parameters than those from visual cues and the PTO. Birds could directly estimate altitude with a barometric measurement by means of their PTO, but with a relatively coarse resolution (ca. $\pm 10\text{m}$). The optimum airspeed V_{mr} is an optimum in relation, not only to the physiology and the morphology of the bird, but also the environmental context (see section 2). Consequently, a bird does not set its flight at a given V_{mr} . We argue it is almost the same thing for altitude, where the environmental context sets its trajectory mainly via its vision. The wind and the airspeed V_{mr} set the bird's groundspeed, and visual information coming from the ground (or sea) can help it to set its altitude up to hundreds of meters.

We tried to represent below the effect on ventral optic flow of a 10m-altitude resolution during a gull's cruise flight, such as a 10m-altitude resolution has been observed in pigeons' PTO [36, 50]. We consider here a gull flying at a groundspeed of 10.9m/s at an altitude of 25m, which generates a ventral optic flow of 25°/s (Fig. 9). The PTO will inform it that it is flying at 25m ± 10m, which corresponds in motion vision at a 25°/s ± 16.6°/s ventral optic flow range (Fig. 9). However, LM neurons are able to measure a ventral optic flow from 0.125°/s to 34°/s with a resolution of ca. 1 spike/s per °/s [75, 76]. Consequently, we can assume the gull's motion vision is able to inform it at a 25°/s ± 1°/s, ensuring it to stabilise its altitude at 25m ± 1m without 10m-oscillations as would result if based on PTO.

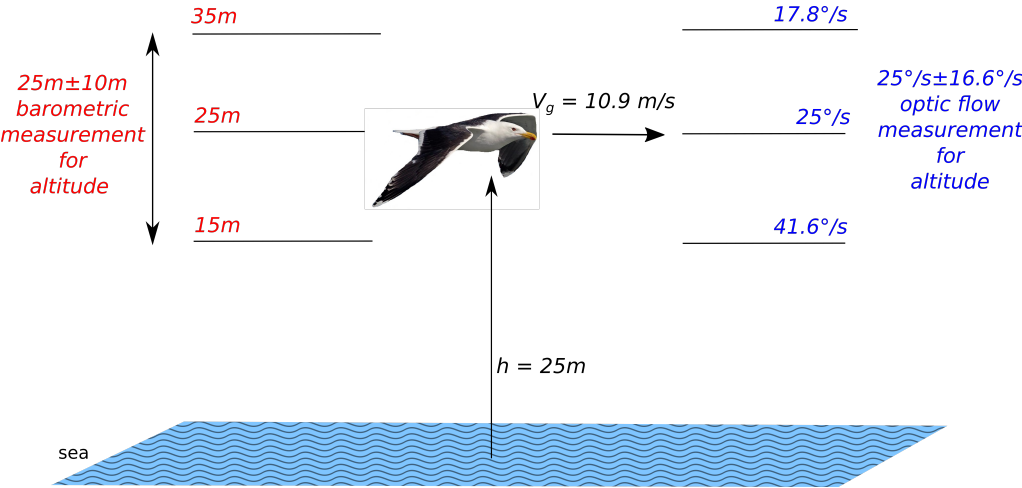


Figure 9. Altitude sensing in seabirds either by barometric pressure measurement or optic flow measurement at an altitude of 25m and a groundspeed of 10.9m/s generating a ventral optic flow of 25°/s.

The GPS accuracy is ca. 2.5m, which is above the optic flow-based altitude control accuracy of ca. 1m at 25m. Consequently in cruise flight, we didn't observe any bird's vertical oscillation in GPS data. However, at higher altitude, if a gull is flying at 15m/s at 78m altitude, it will perceive an optic flow of 11°/s. With a 1°/s resolution in optic flow measurement, it should be able to estimate its altitude at $78\text{m} \pm 6\text{m}$, which puts the motion vision's altitude resolution closer the PTO's altitude resolution. Consequently, over hundreds of meters in altitude, birds cannot maintain a constant altitude with respect to their ventral optic flow's objective, but will show small altitude oscillations, and neither will the bird be able to adapt its airspeed according to winds (also called wind flexibility behaviour, see [46]).

(f) Can birds use their binocular vision for depth perception and then to control their altitude?

G. Martin ([42] and [44] -chapters 8 & 9-) explained that the primary role of binocular vision in birds is for the control of the bill tip. In addition, the binocular visual field of a seabird (the skimmer) is oriented around its bill tip and not really toward the ground [45]. Most of the seabirds have a maximum binocular field width in the 15° – 30° range (about 120° in humans), which is limited, suggesting that binocular vision plays only a minor role in seabirds' flight control system [42].

In particular, the state of scientific knowledge about the role of binocular vision in the distance perception and flight control of birds has been summarised [42] : "Exactly how birds do control their behaviour when landing is still not clear, but Davies and Green (1994) [13] suggest that a

complex of multiple sources of information that may provide birds with distance cues to close objects are available to birds when using only one eye and thus do not involve binocularity."

Our results revive the ecological perceptual approach conducted initially by Davies and Green (1994) [13] in the light of the latest results on the direct use of optic flow observed in flying insects and in bio-inspired robotics [19] as well as in the light of the latest knowledge acquired on birds.

(g) Effect of waves on the optic flow pattern

The flight model assumes that the sea-surface, over which the gulls fly, provides a stationary reference frame: no data are currently available on the wave speed. Therefore, the optic flow experienced by the gulls is solely modeled as a function of their own movement (groundspeed and altitude). Previous studies on bird navigation over water suggest that the seascape (or more specifically the wavescape) is not a fixed reference frame [1], as the wave patterns move, usually in roughly the same direction as the wind but at a slower speed. Therefore the perceived optic flow will be different than the physical optic flow. Alerstam & Petterson (1976) suggested that the motion of the wave scape allows birds to only partially compensate for wind-drift over the sea [3], thus presumably a similar constraint may apply to using the ventral optic flow for control of flight altitude.

Overall, the wave pattern will reduce the adjustment of altitude if a fixed optic flow set-point was used, as under headwinds perceived optic flow will be higher than otherwise, i.e. even as groundspeed approaches zero there will still be a perceived optic flow if the wavescape is moving, which would lead to higher flight altitudes than expected. While under tailwinds optic flow is somewhat reduced, as the sea surface pattern will be moving in the same direction as the bird, and hence lower than expected flight altitudes would result. The wave pattern distorts the ventral optic flow perceived: such disturbances could be added to the flight model once data or a methodology of how to obtain wave pattern becomes available.

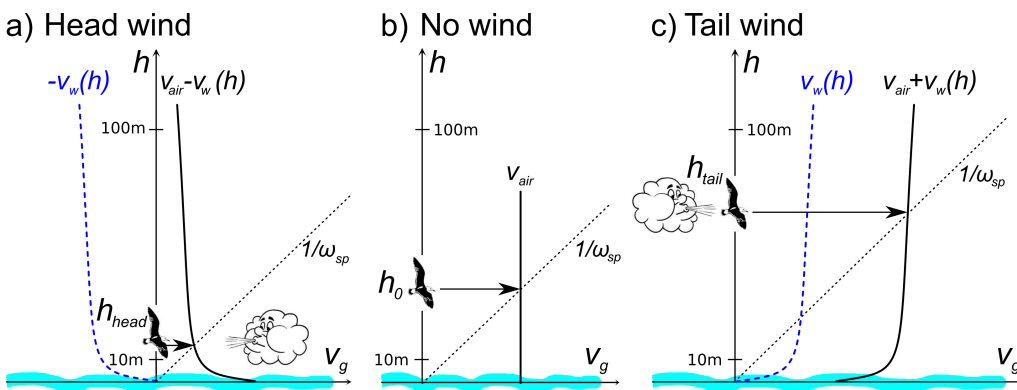


Figure 10. Gull's speed and altitude for three different wind scenarios under the hypothesis that the gull adjusts its vertical thrust to maintain a constant ventral optic flow. The dotted black line $\frac{1}{\omega_{sp}}$ indicates the set of possible pairs of altitudes and groundspeeds allowed by the ventral optic flow regulation hypothesis. (a) In the presence of a head wind, given that the wind speed increases with the altitude, the groundspeed profile $V_{air} - V_w(h)$ intersects the dotted black line $\frac{1}{\omega_{sp}}$ at a lower altitude h_{head} than in absence of wind. (b) In the absence of wind, the ground speed and hence the altitude depend only on the airspeed produced by the agent: the vertical line $V_g = V_{air}$ intersects the line $\frac{1}{\omega_{sp}}$ at the altitude h_0 . (c) In the presence of a tail wind, the ground speed profile $V_{air} + V_w(h)$ intersects the dotted black line $\frac{1}{\omega_{sp}}$ at a greater altitude h_{tail} than in absence of wind. Modified from [61].

However, for optic flow to be useful ripples above the sea are essential to form a textured surface. In fact, it was observed by Heran & Lindauer (1963) that a great number of honeybees plunged into the water when the water surface was mirror smooth [29]. An altitude control

system based solely on a ventral optic flow regulation irrevocably pulls any flying animal down whenever its eye fails to measure an optic flow [19]. This did not happen in honeybees when the water surface was rippled [29, 68] or when a floating bridge provided a visual contrast [29].

At this level of reasoning, we may wonder if the visual pattern produced by waves was textured enough during the gulls' flights for an optic flow field to be perceived. To investigate this, knowing that the average significant wave height of the Baltic Sea in 1991–2015 was in the range 0.44–1.94 m [37], which corresponds to a Beaufort number of 3 (gentle breeze, mean wind speed equivalent from 3.4 m/s to 5.4 m/s) to 4 (moderate breeze, mean wind speed equivalent from 5.5 m/s to 7.9 m/s) [6]. We deduce that gulls could see scattered or fairly frequent white-crested waves at an effective height of 10 m above the sea level. However for Beaufort numbers from 0 to 2, the sea has a smooth appearance, which makes for poor visual conditions to perceive an optic flow field. Interestingly, the wind conditions corresponding to a Beaufort number from 3 to 4 fit not only with the wind conditions of gulls in flight (Fig. S21), but also with their altitude (see page 166 in [18]). We can conclude that wind is an important parameter to generate an optic flow field cue, and to help gulls to control their flight above the sea.

The spatial acuity of seabirds can be more than four times lower than that in humans [47], with a maximum spatial acuity of about 60 cycles/degree in humans. Moreover, in seabirds, rods are evenly distributed across the entire retina [16], which allow them to conveniently detect the optic flow coming from the sea.

We conclude that the optic flow field is potentially the major visual cue used by seabirds to control their altitude above the sea.

(h) Optic flow set-point: differences between honeybees and gulls

There are a number of differences in flight behaviours expressed by birds and flying insects [4]. Typically, the average maximum airspeed of honeybees is approximately 7.5 m/s with a minimum power speed of their power U-curve at 3.3 m/s [48]. In free-flight natural conditions, honeybees have been observed to fly from 3.3 m/s to 5.1 m/s [48]. However, lesser black-backed gulls typically fly at an airspeed in natural offshore conditions at an average $12.3 \text{ m/s} \pm 2 \text{ m/s}$ (see [18], page 166) with a minimum power speed of their power U-curve at 9.3 m/s (computed for lesser black-backed gull, see [28]). Hence, lesser black-backed gulls can fly 3 times faster than honeybees by comparing their minimum power speed.

In honeybees, average maximal flight height is about 2.5 m over natural terrain [17, 29]. In general, lesser black-backed gulls fly at an altitude over sea of up to 130 m with a distribution of $31 \text{ m} \pm 29 \text{ m}$ on average (see [18], pages 166–167) during foraging flights. We conclude that lesser black-backed gulls fly much higher than honeybees during foraging flights, which reduces optic flow emanating from the sea.

Consequently, we can conclude from these two last points that the ventral optic-flow set-point of lesser black-backed gulls is much lower than that typically experienced by honeybees, knowing that the ventral optic-flow set-point of honeybees is close to $200^\circ/\text{s}$. Our statistical analysis estimates that the ventral optic-flow set-point of lesser black-backed gulls is close to $25^\circ/\text{s}$ on average (see section (a)), which is a detectable value by the gulls' visual system [42, 43, 44]. A recent review indicates that pigeons' fast LM neurons (pretectal nucleus lentiformis mesencephali) respond to optic flow stimuli of their preferred backward direction (front to back visual stimuli: temporal to nasal on the retina) in this same angular velocities range [76].

6. Conclusion

A mathematical model of optic flow-based offshore takeoff control system in lesser black-backed gulls was developed in this study to understand what visual cue can be used by seabirds to control their takeoff and to cruise over a sea surface. This mathematical model introduced an optic flow set-point parameter, which aims to be maintained constant by seabirds during take-off manoeuvres and cruising foraging flights. Besides, the model takes into account the bird's

individual morphology through its elevation dynamics. Finally, both analyses on the takeoff time-series and the full dataset support the ventral optic flow regulation hypothesis in a consistent manner.

We conclude that the optic-flow regulation principle allows seabirds to control their altitude over sea at low flight altitudes without having to measure their current altitude directly by another method. To do this, they just have to measure the optic flow perceived from the sea to adjust their vertical thrust in order to maintain the ventral optic flow at a given value, called the optic flow set-point, as previously suggested for flying insects [19, 61]. According to both the airspeed and altitude ranges of lesser black-backed gulls measured during flight in their natural environment, we demonstrate that gulls could control their altitude by regulating the ventral optic flow at a value of $25^\circ/s$ on average, allowing them to fly jointly up to 130 m in altitude at a groundspeed up to 20 m/s, while maintaining visual contact with the sea. The introduction of this asymptotic proportionality relationship for birds also accounts very nicely for the transient altitude response during takeoff. Overall, gulls need such accurate altitude control based on optic flow to optimize their energetic effort irrespectively of favorable or unfavorable unknown wind conditions while being robust to ground disturbances such as relief. This study cannot claim that "optic flow" alone controls altitude in birds, but we think that multiple sensory systems with different resolution are implicated in the birds' altitude control comprising visual cues and PTO. We hope this study will promote questions and investigations in other birds species.

Authors' contributions

JRS, FR, TJE and AH developed the modelling; JRS ran the models on Matlab software; TJE and SÅ tagged the gulls and collected the data; JRS, TJE and FR analysed the modelling results; JSB provided the tracking system; FR and AH supervised the collaboration; FR drew figs 1 and 10; TJE drew table S2, figs 2 and 3; JRS drew table S1, figs 4, 5, 7, 8, 9 and S3-S20; TJE, JRS and FR drew fig 6; JRS wrote the first draft of the paper; all authors prepared and revised the manuscript.

Acknowledgement

French financial support was provided by a project grant to FR from the CNRS PEPS Avimod (Exomod Program). FR and JRS were also supported by Aix Marseille Université and CNRS (Life Science; Information Science, and Engineering Science and Technology). Financial support was via project grants to SÅ and AH from the Swedish Research Council (621-2007-5930; 621-2010-5584, 621-2013-4361, 621-2012-3585) and Lund University, and a Linnaeus grant from the Swedish Research Council (349-2007-8690) to the Centre for Animal Movement Research (CAnMove) and Lund University. Field work was partly supported by WWF Sweden. UvA-BiTS is facilitated by infrastructures for eScience, developed with support of the NLeSC (<http://www.esciencecenter.com/>) and LifeWatch, carried out on the Dutch national e-infrastructure with support of SURF Foundation. For assistance during fieldwork we thank the whole Baltic Seabird Group team, especially: Olof Olsson, Jonas Hentati-Sundberg, Per-Arvid Berglund, Aron Hejdström, Martina Kadin, Natalie Isaksson, and Rebecca Young. We would like to thank Prof. Maan El Badaoui El Najjar (Univ. of Lille) for his fruitful comments during this analysis.

References

- 1 Åkesson, S. & Hedenström, A. 2007 How migrants get there: migratory performance and orientation. *AIBS Bulletin*, 57(2), 123–133.
- 2 Alerstam, T. 1990 *Bird migration*. Cambridge University Press.
- 3 Alerstam, T. & Pettersson, S.-G. 1976 Do birds use waves for orientation when migrating across the sea? *Nature*, 259(5540), 205–207.
- 4 Altshuler, D. L. & Srinivasan, M. V. 2018 Comparison of visually guided flight in insects and birds. *Frontiers in neuroscience*, 12, 157.

- 5 Baker, C. V., O'Neill, P. & McCole, R. B. 2008 Lateral line, otic and epibranchial placodes: developmental and evolutionary links? *Journal of Experimental Zoology Part B: Molecular and Developmental Evolution*, **310**(4), 370–383.
- 6 Beaufort, F. 1805 Beaufort wind scale. *British Rea-Admiral*.
- 7 Bhagavatula, P. S., Claudianos, C., Ibbotson, M. R. & Srinivasan, M. V. 2011 Optic flow cues guide flight in birds. *Current Biology*, **21**(21), 1794–1799.
- 8 Blake, R. 1985 A model of foraging efficiency and daily energy budget in the black skimmer (*rynchops nigra*). *Canadian journal of zoology*, **63**(1), 42–48.
- 9 Bouten, W., Baaij, E. W., Shamoun-Baranes, J. & Camphuysen, K. C. 2013 A flexible gps tracking system for studying bird behaviour at multiple scales. *Journal of Ornithology*, **154**(2), 571–580.
- 10 Breuner, C. W., Sprague, R. S., Patterson, S. H. & Woods, H. A. 2013 Environment, behavior and physiology: do birds use barometric pressure to predict storms? *Journal of Experimental Biology*, **216**(11), 1982–1990.
- 11 Coulson, J. C., Thomas, C. S., Butterfield, J. E. L., Duncan, N., Monaghan, P. & Shedden, C. The use of head and bill length to sex live gulls larvae. *Ibis*, **125**(4), 549–557. (doi:10.1111/j.1474-919X.1983.tb03148.x)
- 12 Davies, M. & Green, P. 1990 Optic flow-field variables trigger landing in hawk but not in pigeons. *Naturwissenschaften*, **77**(3), 142–144.
- 13 Davies, M. & Green, P. 1994 Multiple sources of depth information: an ecological approach. In *Perception and motor control in birds*, pp. 339–356. Springer.
- 14 Dee, D. P., Uppala, S. M., Simmons, A. J., Berrisford, P., Poli, P., Kobayashi, S., Andrae, U., Balmaseda, M. A., Balsamo, G. *et al.* 2011 The ERA-Interim reanalysis: configuration and performance of the data assimilation system. *Quarterly Journal of the Royal Meteorological Society*, **137**(656), 553–597. (doi:10.1002/qj.828)
- 15 Dodge, S., Bohrer, G., Weinzierl, R., Davidson, S. C., Kays, R., Douglas, D., Cruz, S., Han, J., Brandes, D. *et al.* 2013 The environmental-data automated track annotation (Env-DATA) system: linking animal tracks with environmental data. *Movement Ecology*, **1**(1), 3. (doi:10.1186/2051-3933-1-3)
- 16 Emond, M., McNeil, R., Cabana, T., Guerra, C. & Lachapelle, P. 2006 Comparing the retinal structures and functions in two species of gulls (*larus delawarensis* and *larus modestus*) with significant nocturnal behaviours. *Vision research*, **46**(18), 2914–2925.
- 17 Esch, H. & Burns, J. 1996 Distance estimation by foraging honeybees. *Journal of Experimental Biology*, **199**(1), 155–162.
- 18 Evans, T. J. 2017 *Across landscapes and seascapes : The movement ecology of diving and flying guillemots and gulls during breeding*. PhD thesis, Lund University, Faculty of Science, Department of Biology.
- 19 Franceschini, N., Ruffier, F. & Serres, J. 2007 A bio-inspired flying robot sheds light on insect piloting abilities. *Current Biology*, **17**(4), 329–335.
- 20 Gibson, J. J. 1966 *The senses considered as perceptual systems*. Houghton Mifflin.
- 21 Goller, B. & Altshuler, D. L. 2014 Hummingbirds control hovering flight by stabilizing visual motion. *Proceedings of the National Academy of Sciences*, **111**(51), 18375–18380.
- 22 Greenewalt, C. H. 1962 Dimensional relationships for flying animals. *Smithsonian miscellaneous collections*, **144**, 1–46.
- 23 Griffin, D. R. 1969 The physiology and geophysics of bird navigation. *The Quarterly Review of Biology*, **44**(3), 255–276.
- 24 Griffiths, R., Double, M. C., Orr, K. & Dawson, R. J. G. 1998 A DNA test to sex most birds. *Molecular Ecology*, **7**(8), 1071–1075. (doi:10.1046/j.1365-294x.1998.00389.x)
- 25 Hedenström, A. 2003 Twenty-three testable predictions about bird flight. In *Avian migration*, pp. 563–582. Springer.
- 26 Hedenström, A. & Åkesson, S. 2017 Adaptive airspeed adjustment and compensation for wind drift in the common swift: Differences between day and night. *Animal Behaviour*, **127**, 117–123.
- 27 Hedenstrom, A. & Alerstam, T. 1995 Optimal flight speed of birds. *Philosophical Transactions of the Royal Society of London B: Biological Sciences*, **348**(1326), 471–487.

- 28 Heerenbrink, M. K., Johansson, L. & Hedenström, A. 2015 Power of the wingbeat: modelling the effects of flapping wings in vertebrate flight. *Proceedings of the Royal Society A*, **471**(2177), 20140952.
- 29 Heran, H. & Lindauer, M. 1963 Windkompensation und seitenwindkorrektur der bienen beim flug über wasser. *Zeitschrift für vergleichende Physiologie*, **47**(1), 39–55.
- 30 Holbrook, R. I. & de Perera, T. B. 2011 Fish navigation in the vertical dimension: can fish use hydrostatic pressure to determine depth? *Fish and Fisheries*, **12**(4), 370–379.
- 31 Hsu, S., Meindl, E. A. & Gilhousen, D. B. 1994 Determining the power-law wind-profile exponent under near-neutral stability conditions at sea. *Journal of Applied Meteorology*, **33**(6), 757–765.
- 32 Irwin, J. S. 1979 A theoretical variation of the wind profile power-law exponent as a function of surface roughness and stability. *Atmospheric Environment (1967)*, **13**(1), 191 – 194. (doi:https://doi.org/10.1016/0004-6981(79)90260-9)
- 33 Isaksson, N., Evans, T. J., Shamoun-Baranes, J. & Åkesson, S. 2016 Land or sea? Foraging area choice during breeding by an omnivorous gull. *Movement Ecology*, **4**, 11. (doi:10.1186/s40462-016-0078-5)
- 34 Katzir, G., Schechtman, E., Carmi, N. & Weihs, D. 2001 Head stabilization in herons. *Journal of Comparative Physiology A*, **187**(6), 423–432.
- 35 Kogure, Y., Sato, K., Watanuki, Y., Wanless, S. & Daunt, F. 2016 European shags optimize their flight behavior according to wind conditions. *Journal of Experimental Biology*, **219**(3), 311–318.
- 36 Kreithen, M. L. & Keeton, W. T. 1974 Detection of changes in atmospheric pressure by the homing pigeon, *columba livia*. *Journal of comparative physiology*, **89**(1), 73–82.
- 37 Kudryavtseva, N. & Soomere, T. 2017 Satellite altimetry reveals spatial patterns of variations in the baltic sea wave climate. *arXiv preprint arXiv:1705.01307*.
- 38 Lee, D. N. & Kalmus, H. 1980 The optic flow field: the foundation of vision. *Philosophical Transactions of the Royal Society of London B: Biological Sciences*, **290**(1038), 169–179.
- 39 Lee, D. N. & Reddish, P. E. 1981 Plummeting gannets: a paradigm of ecological optics. *Nature*, **293**(5830), 293–294.
- 40 Lee, D. N., Reddish, P. E. & Rand, D. 1991 Aerial docking by hummingbirds. *Naturwissenschaften*, **78**(11), 526–527.
- 41 Liechti, F. 2006 Birds: blowin? by the wind? *Journal of Ornithology*, **147**(2), 202–211. (doi:10.1007/s10336-006-0061-9)
- 42 Martin, G. R. 2009 What is binocular vision for? a birds' eye view. *Journal of Vision*, **9**(11), 14–14.
- 43 Martin, G. R. 2011 Understanding bird collisions with man-made objects: a sensory ecology approach. *Ibis*, **153**(2), 239–254.
- 44 Martin, G. R. 2017 *The sensory ecology of birds*. Oxford University Press.
- 45 Martin, G. R., Mcneil, R. & Rojas, L. M. 2007 Vision and the foraging technique of skimmers (ryncopidae). *Ibis*, **149**(4), 750–757.
- 46 McLaren, J. D., Shamoun-Baranes, J., Camphuysen, C. & Bouten, W. 2016 Directed flight and optimal airspeeds: homeward-bound gulls react flexibly to wind yet fly slower than predicted. *Journal of Avian Biology*, **47**(4), 476–490.
- 47 Mitkus, M., Nevitt, G. A., Danielsen, J. & Kelber, A. 2016 Vision on the high seas: spatial resolution and optical sensitivity in two procellariiform seabirds with different foraging strategies. *Journal of Experimental Biology*, **219**(21), 3329–3338.
- 48 Nachtigall, W., Hanauer-Thieser, U. & Mörz, M. 1995 Flight of the honey bee vii: metabolic power versus flight speed relation. *Journal of Comparative Physiology B: Biochemical, Systemic, and Environmental Physiology*, **165**(6), 484–489.
- 49 Nakayama, K. & Loomis, J. 1974 Optical velocity patterns, velocity-sensitive neurons, and space perception: a hypothesis. *Perception*, **3**(1), 63–80.
- 50 O'neill, P. 2013 Magnetoreception and baroreception in birds. *Development, growth & differentiation*, **55**(1), 188–197.
- 51 Orians, G. H. & Pearson, N. E. On the theory of central place foraging. In *Analysis of ecological systems*. ohio state university press, columbus, pp. 155–177.

- 52 Pennycuick, C. 1975 Mechanics of flight. *Avian biology*, **5**, 1–75.
- 53 Pennycuick, C. J. 1978 Fifteen Testable Predictions about Bird Flight. *Oikos*, **30**(2), 165–176. (doi:10.2307/3543476)
- 54 Pennycuick, C. J. 1989 *Bird flight performance*. Oxford University Press.
- 55 Pennycuick, C. J. 2002 Gust soaring as a basis for the flight of petrels and albatrosses (Procellariiformes). *Avian Science*, **2**(1), 1–12.
- 56 Pennycuick, C. J. 2008 *Modelling the flying bird*, vol. 5. Elsevier.
- 57 Pete, A. E., Kress, D., Dimitrov, M. A. & Lentink, D. 2015 The role of passive avian head stabilization in flapping flight. *Journal of The Royal Society Interface*, **12**(110), 20150508.
- 58 Rayleigh 1883 The soaring of birds. *Nature*, **27**(701), 534–535. (doi:10.1038/027534a0)
- 59 Richardson, P. L. 2011 How do albatrosses fly around the world without flapping their wings? *Progress in Oceanography*, **88**(1), 46–58.
- 60 Ros, I. G. & Biewener, A. A. 2016 Optic flow stabilizes flight in ruby-throated hummingbirds. *Journal of Experimental Biology*, **219**(16), 2443–2448.
- 61 Ruffier, F. & Franceschini, N. 2005 Optic flow regulation: the key to aircraft automatic guidance. *Robotics and Autonomous Systems*, **50**(4), 177–194.
- 62 Sachs, G., Traugott, J., Nesterova, A. P., Dell’Omo, G., Kümmeth, F., Heidrich, W., Vyssotski, A. L. & Bonadonna, F. 2012 Flying at no mechanical energy cost: disclosing the secret of wandering albatrosses. *PLoS One*, **7**(9), e41449.
- 63 Schiffner, I. & Srinivasan, M. V. 2016 Budgerigar flight in a varying environment: flight at distinct speeds? *Biology Letters*, **12**(6), 20160221.
- 64 Serres, J. R. & Ruffier, F. 2017 Optic flow-based collision-free strategies: From insects to robots. *Arthropod Structure & Development*, **46**(5), 703–717.
- 65 Shamoun-Baranes, J., Liechti, F. & Vansteelant, W. M. 2017 Atmospheric conditions create freeways, detours and tailbacks for migrating birds. *Journal of Comparative Physiology A*, pp. 1–21.
- 66 Shamoun-Baranes, J., Van Loon, E., Alon, D., Alpert, P., Yom-Tov, Y. & Leshem, Y. 2006 Is there a connection between weather at departure sites, onset of migration and timing of soaring-bird autumn migration in israel? *Global Ecology and Biogeography*, **15**(6), 541–552.
- 67 Spivey, R., Stansfield, S. & Bishop, C. 2014 Analysing the intermittent flapping flight of a manx shearwater, puffinus puffinus, and its sporadic use of a wave-meandering wing-sailing flight strategy. *Progress in Oceanography*, **125**, 62–73.
- 68 Tautz, J., Zhang, S., Spaethe, J., Brockmann, A., Si, A. & Srinivasan, M. 2004 Honeybee odometry: performance in varying natural terrain. *PLoS Biology*, **2**(7), e211.
- 69 Taylor, G. K., Holbrook, R. I. & de Perera, T. B. 2010 Fractional rate of change of swim-bladder volume is reliably related to absolute depth during vertical displacements in teleost fish. *Journal of The Royal Society Interface*, **7**(50), 1379–1382.
- 70 Thaxter, C. B., Ross-Smith, V. H., Clark, J. A., Clark, N. A., Conway, G. J., Marsh, M., Leat, E. H. & Burton, N. H. 2014 A trial of three harness attachment methods and their suitability for long-term use on Lesser Black-backed Gulls and Great Skuas. *Ringing & Migration*, **29**(2), 65–76. (doi:10.1080/03078698.2014.995546)
- 71 von Bartheld, C. S. & Giannessi, F. 2011 The paratympanic organ: a barometer and altimeter in the middle ear of birds? *Journal of Experimental Zoology Part B: Molecular and Developmental Evolution*, **316**(6), 402–408.
- 72 Weimerskirch, H., Guionnet, T., Martin, J., Shaffer, S. A. & Costa, D. P. 2000 Fast and fuel efficient? Optimal use of wind by flying albatrosses. *Proceedings of the Royal Society B: Biological Sciences*, **267**(1455), 1869–1874. (doi:10.1098/rspb.2000.1223)
- 73 Whiteside, T. C. & Samuel, G. 1970 Blur zone. *Nature*, **225**(5227), 94–95.
- 74 Wilson, J. A. 1975 Sweeping flight and soaring by albatrosses. *Nature*, **257**(5524), 307. (doi:10.1038/257307a0)
- 75 Wylie, D., Bischof, W. & Frost, B. 1998 Common reference frame for neural coding of translational and rotational optic flow. *Nature*, **392**(6673), 278.
- 76 Wylie, D. R., Gutiérrez-Ibáñez, C., Gaede, A. H., Altshuler, D. L. & Iwaniuk, A. N. 2018 Visual-cerebellar pathways and their roles in the control of avian flight. *Frontiers in Neuroscience*, **12**, 223. (doi:10.3389/fnins.2018.00223)

Optic flow cues help explain altitude control over sea in freely flying gulls

Julien R. Serres, Thomas J. Evans, Susanne Åkesson, Olivier Duriez, Judy Shamoun-Baranes, Franck Ruffier, and Anders Hedenström.

h	0	$h_{ref} \cdot \left(\frac{\omega_{sp}}{V_{ref} \cdot \alpha} \right)^{\frac{1}{\alpha-1}}$	$+\infty$
$\frac{\partial f}{\partial h}$	+	0	-
$f(h)$	$V_{air} > 0$	\hat{f}	0 $\rightarrow -\infty$

Table S1: Variation table of the function f described by equation (2.9). There exists only a unique altitude h enabling $f(h) = 0$.

Bird ID	Number of flights	Number of GPS fixes median \pm MAD	Flight duration tracked (s) median \pm MAD	Time interval (s) median \pm MAD
8111155	44	17 \pm 11.9	1963.5 \pm 1431.5	123.2 \pm 86.2
8111176	31	41 \pm 34.1	2366 \pm 2071.2	114.7 \pm 19.0
8111177	30	25 \pm 14.1	2266 \pm 1439.6	120.9 \pm 34.1
8111250	31	24 \pm 20.8	1712 \pm 1254.3	122.4 \pm 143.7
8114313	11	28 \pm 32.6	1136 \pm 883.6	180.6 \pm 222.4
8114314	5	10 \pm 8.9	1393 \pm 1344.7	154.6 \pm 60.6
8114315	34	13.5 \pm 14.8	1689.5 \pm 853.2	142.9 \pm 189.7
8114316	14	54 \pm 71.9	1146.5 \pm 563.4	23.7 \pm 17.1
8114317	3	53 \pm 13.3	640 \pm 7.4	25.8 \pm 14.4
8114318	9	109 \pm 65.2	1240 \pm 889.6	18.2 \pm 10.2
8114345	48	17 \pm 12.6	2625.5 \pm 1733.9	196.3 \pm 165.2
8114347	21	56 \pm 50.4	2645 \pm 1642.7	34.1 \pm 30.0
8114348	18	19 \pm 19.3	1816 \pm 1156.4	196.5 \pm 214.6
8114349	1	15 \pm 0	2766 \pm 0	197.2 \pm 0
8114370	14	25.5 \pm 18.5	1903.5 \pm 693.9	139.3 \pm 32.8
8114371	38	45 \pm 29.7	3417 \pm 1993.4	115.4 \pm 39.0

Table S2: Details of flights included in dataset, with the identifier number for each bird (noted Bird ID). For each bird, the number of flights, the number of GPS fixes (in number of points), the flight duration tracked (in seconds), and the time interval (in seconds) are shown with median absolute deviation (MAD) showing variation between flights.

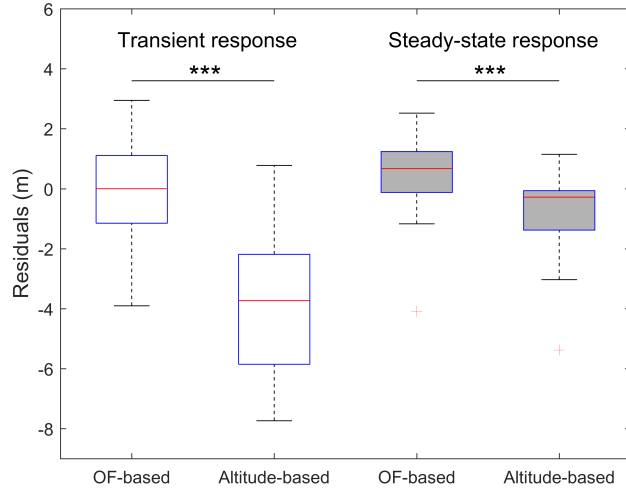


Figure S3: The residuals distribution (in meters) of each model (set of medians in Figs. 8c-d, $n = 27$ for each boxplot) in transient response (white shaded boxes) and in steady-state response (gray shaded boxes). The distributions are presented using classical boxplots showing the median (red line), the 25th and the 75th percentiles (blue box), and the minimum and maximum values (black whiskers). “OF-based” stands for optic flow-based control model and “Altitude-based” stands for altitude control model. The mean of the distribution of the difference between residuals’ distributions is significantly higher than the mean altitude error (2.77 m) of the GPS tracker (Bouten *et al.* 2013) in transient response (one-sided t -test, $n = 27$, $p \ll 0.001$).

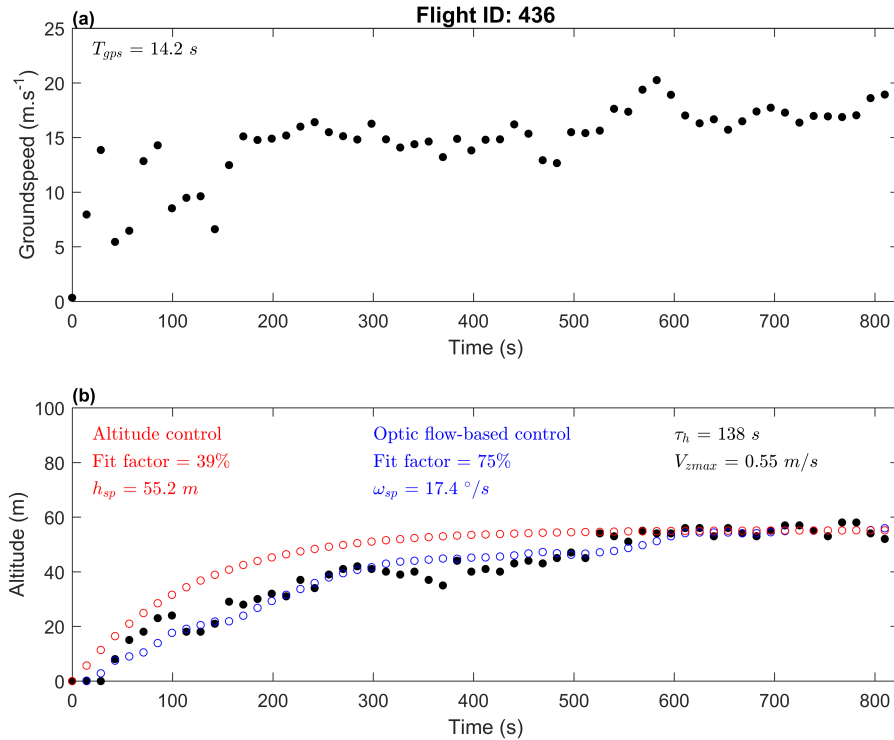


Figure S4: (a) Groundspeed of the gull ID426 tracked with the GPS. (b) Altitude of the gull: black dots represent the GPS data, red dots represent the gull altitude on the basis of an altitude-based control model (fit factor: 39%), and the blue dots represent the gull altitude on the basis of an optic flow-based control model (fit factor: 75%). A significant correlation was observed between groundspeed and altitude of the GPS data ($\rho = 0.71$, $p \ll 0.001$ by Spearman’s test).

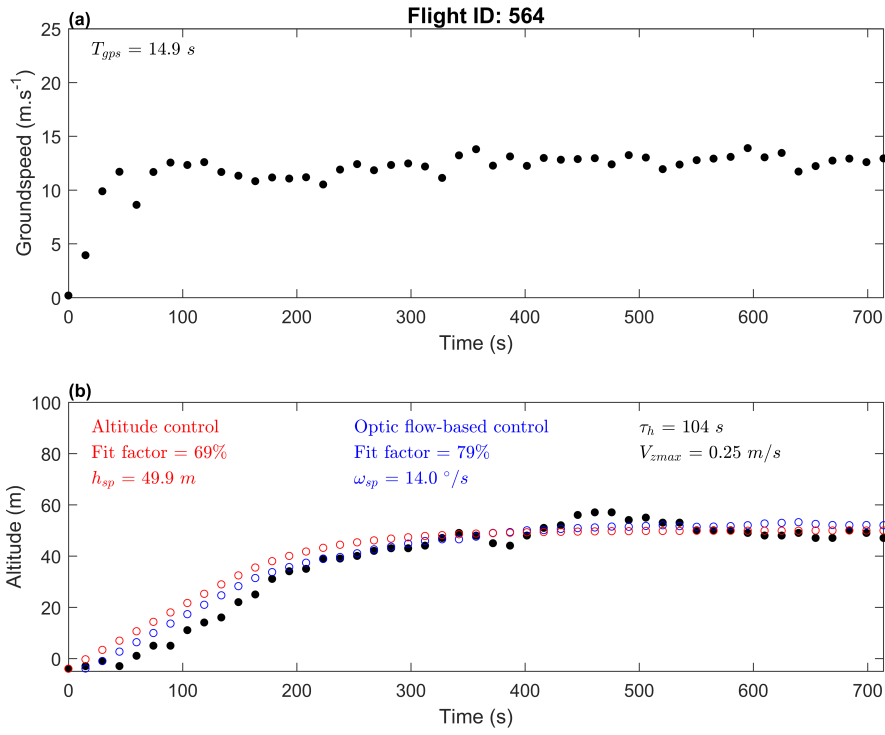


Figure S5: (a) Groundspeed of the gull ID564 tracked with the GPS. (b) Altitude of the gull: black dots represent the GPS data, red dots represent the gull altitude on the basis of an altitude-based control model (fit factor: 69%), and the blue dots represent the gull altitude on the basis of an optic flow-based control model (fit factor: 79%). A significant correlation was observed between groundspeed and altitude of the GPS data ($\rho = 0.68$, $p \ll 0.001$ by Spearman's test).

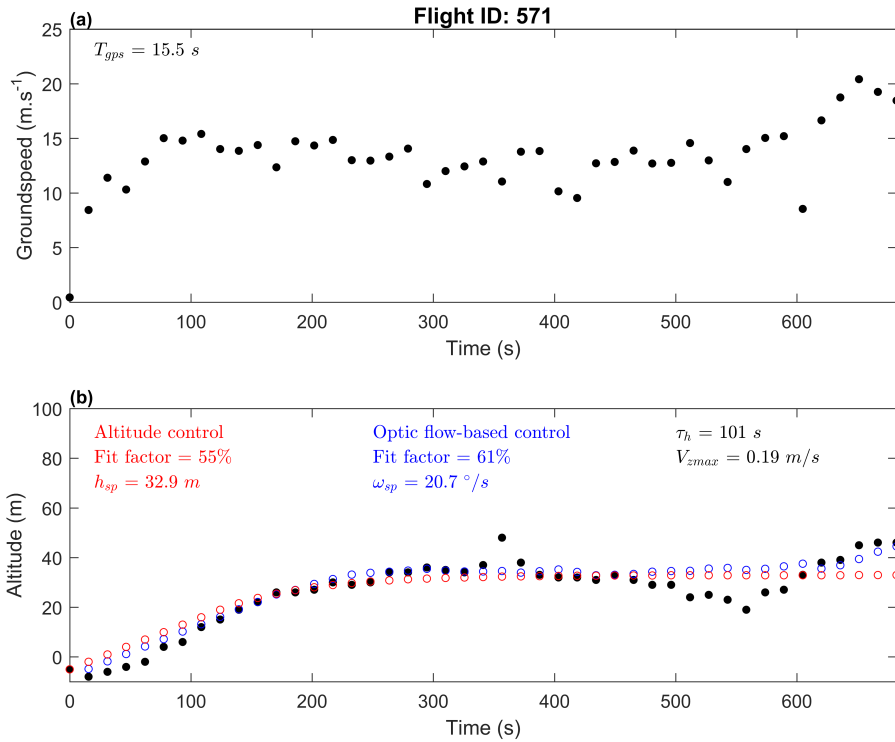


Figure S6: (a) Groundspeed of the gull ID571 tracked with the GPS. (b) Altitude of the gull: black dots represent the GPS data, red dots represent the gull altitude on the basis of an altitude-based control model (fit factor: 55%), and the blue dots represent the gull altitude on the basis of an optic flow-based control model (fit factor: 61%). No correlation was observed between groundspeed and altitude of the GPS data.

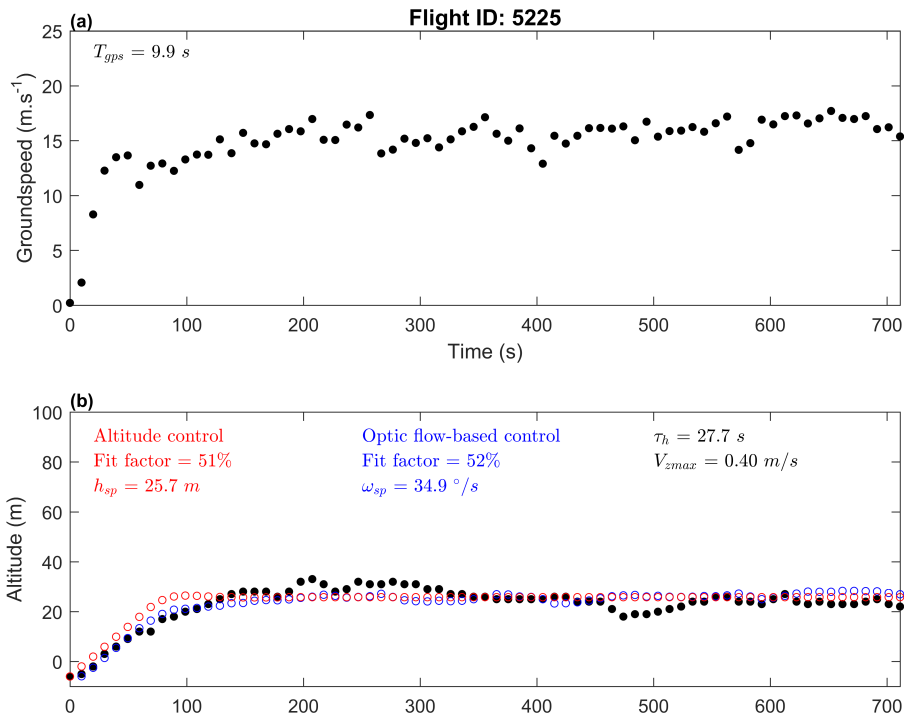


Figure S7:(a) Groundspeed of the gull ID5225 tracked with the GPS. (b) Altitude of the gull: black dots represent the GPS data, red dots represent the gull altitude on the basis of an altitude-based control model (fit factor: 51%), and the blue dots represent the gull altitude on the basis of an optic flow-based control model (fit factor: 52%). A significant correlation was observed between groundspeed and altitude of the GPS data ($\rho = 0.27$, $p \ll 0.001$ by Spearman's test).

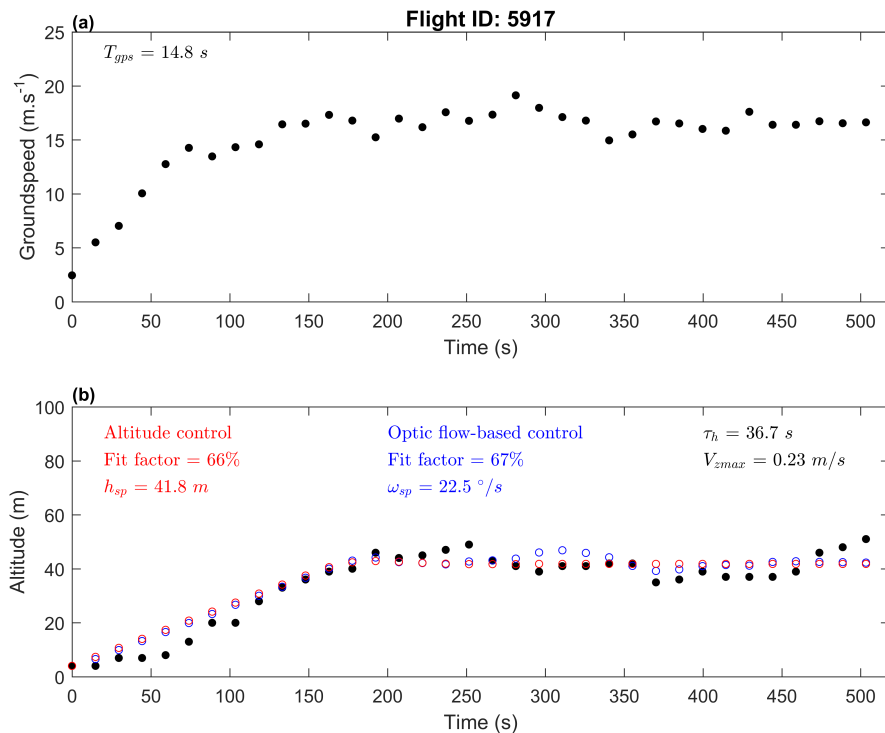


Figure S8: (a) Groundspeed of the gull ID5917 tracked with the GPS. (b) Altitude of the gull: black dots represent the GPS data, red dots represent the gull altitude on the basis of an altitude-based control model (fit factor: 66%), and the blue dots represent the gull altitude on the basis of an optic flow-based control model (fit factor: 67%). A significant correlation was observed between groundspeed and altitude of the GPS data ($\rho = 0.57$, $p \ll 0.001$ by Spearman's test).

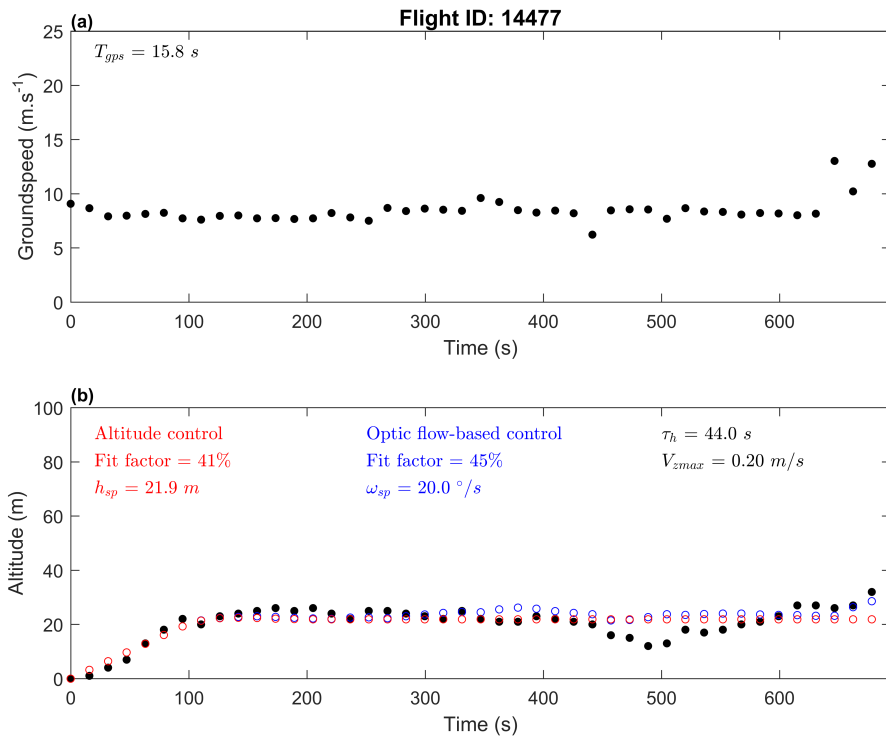


Figure S9: (a) Groundspeed of the gull ID14477 tracked with the GPS. (b) Altitude of the gull: black dots represent the GPS data, red dots represent the gull altitude on the basis of an altitude-based control model (fit factor: 41%), and the blue dots represent the gull altitude on the basis of an optic flow-based control model (fit factor: 45%). No significant correlation was observed between groundspeed and altitude of the GPS data.

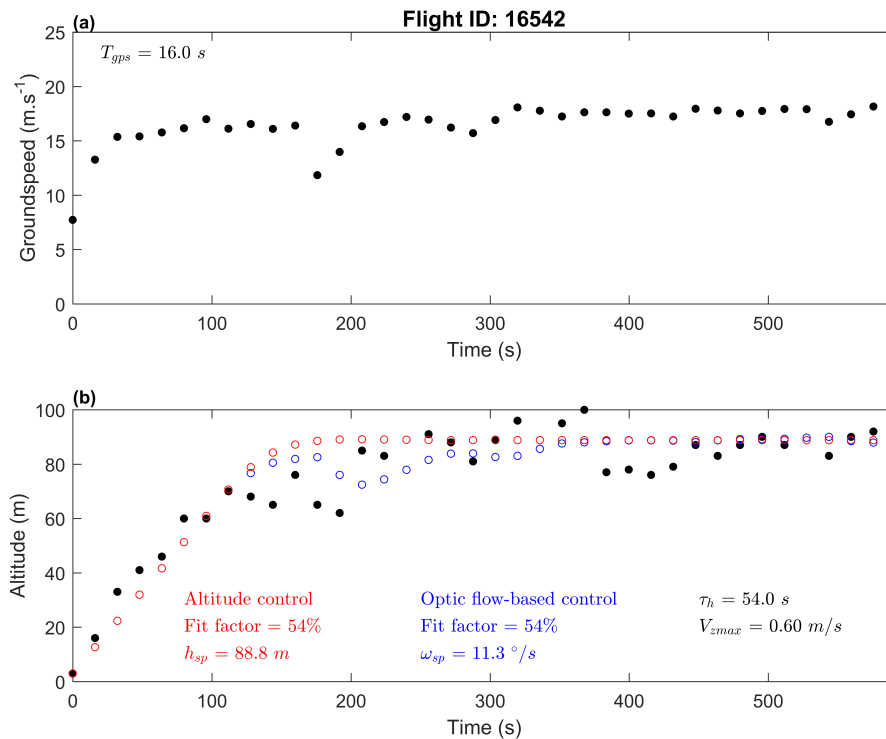


Figure S10: (a) Groundspeed of the gull ID16542 tracked with the GPS. (b) Altitude of the gull: black dots represent the GPS data, red dots represent the gull altitude on the basis of an altitude-based control model (fit factor: 54%), and the blue dots represent the gull altitude on the basis of an optic flow-based control model (fit factor: 54%). No significant correlation was observed between groundspeed and altitude of the GPS data.

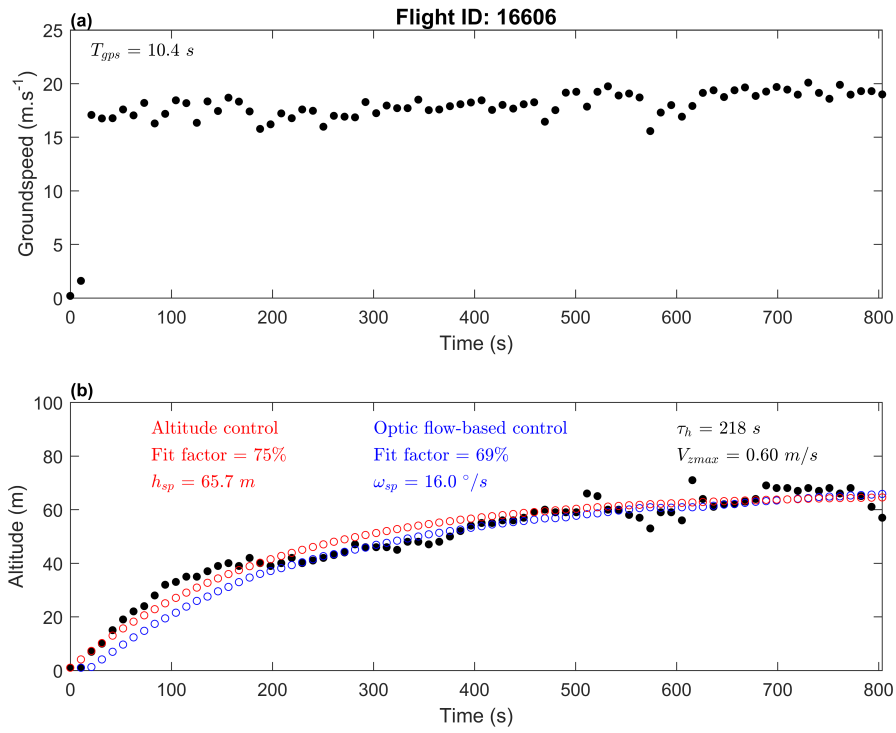


Figure S11: (a) Groundspeed of the gull ID16606 tracked with the GPS. (b) Altitude of the gull: black dots represent the GPS data, red dots represent the gull altitude on the basis of an altitude-based control model (fit factor: 75%), and the blue dots represent the gull altitude on the basis of an optic flow-based control model (fit factor: 69%). A significant correlation was observed between groundspeed and altitude of the GPS data ($\rho = 0.71$, $p \ll 0.001$ by Spearman's test).

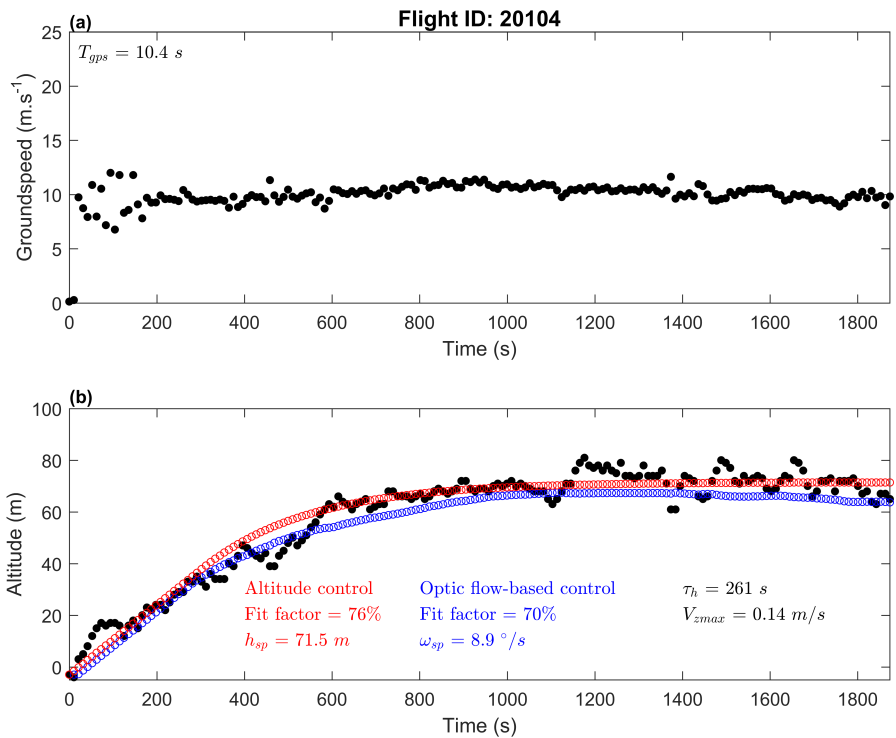


Figure S12: (a) Groundspeed of the gull ID20104 tracked with the GPS. (b) Altitude of the gull: black dots represent the GPS data, red dots represent the gull altitude on the basis of an altitude-based control model (fit factor: 76%), and the blue dots represent the gull altitude on the basis of an optic flow-based control model (fit factor: 70%). A significant correlation was observed between groundspeed and altitude of the GPS data ($\rho = 0.35$, $p \ll 0.001$ by Spearman's test).

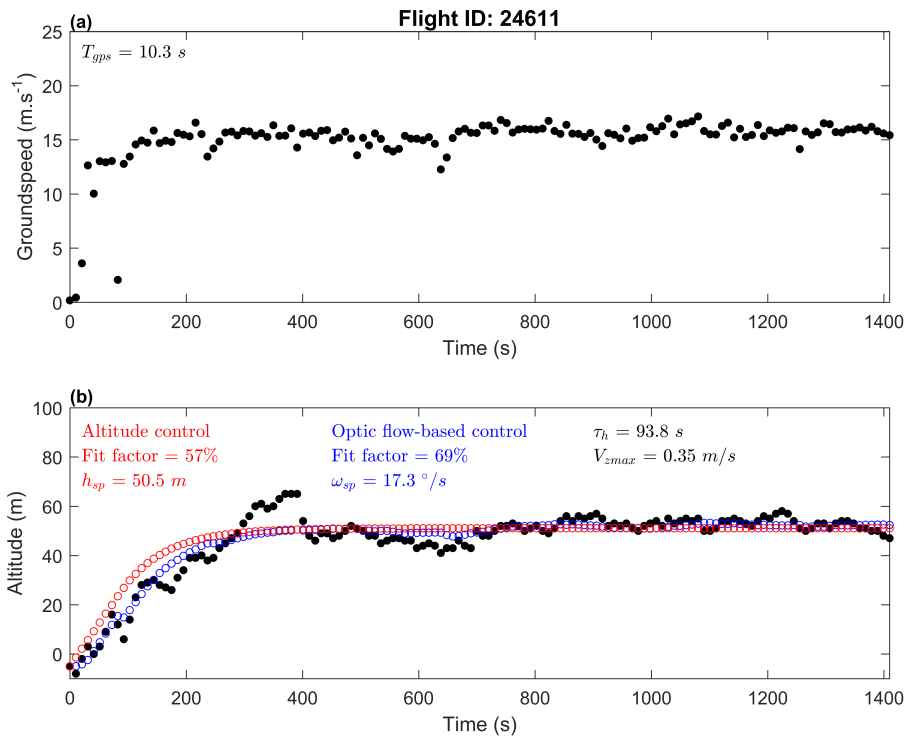


Figure S13: (a) Groundspeed of the gull ID24611 tracked with the GPS. (b) Altitude of the gull: black dots represent the GPS data, red dots represent the gull altitude on the basis of an altitude-based control model (fit factor: 57%), and the blue dots represent the gull altitude on the basis of an optic flow-based control model (fit factor: 69%). A significant correlation was observed between groundspeed and altitude of the GPS data ($\rho = 0.51$, $p \ll 0.001$ by Spearman's test).

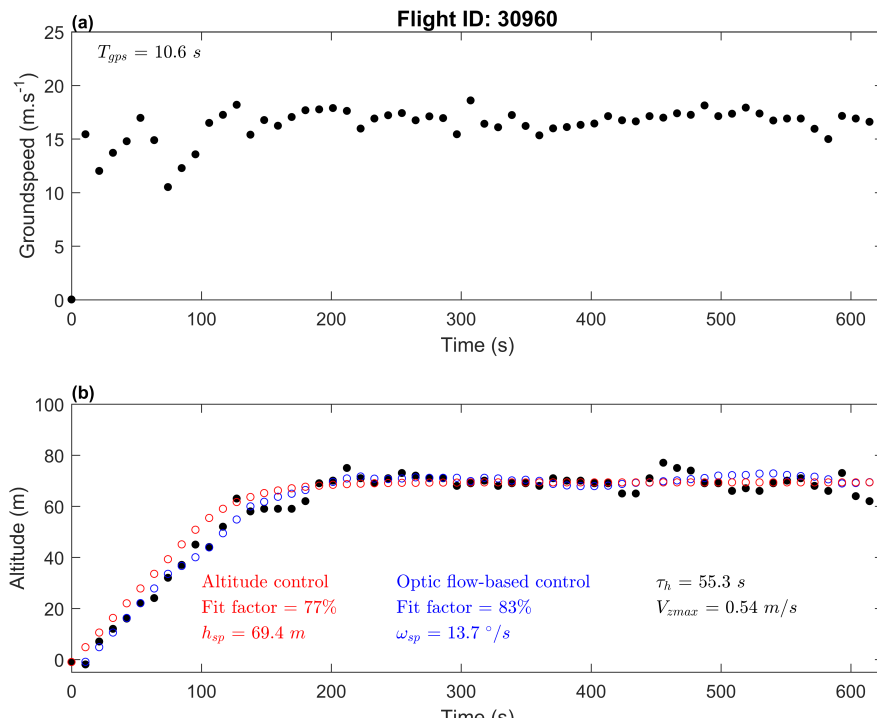


Figure S14 : (a) Groundspeed of the gull ID30960 tracked with the GPS. (b) Altitude of the gull: black dots represent the GPS data, red dots represent the gull altitude on the basis of an altitude-based control model (fit factor: 77%), and the blue dots represent the gull altitude on the basis of an optic flow-based control model (fit factor: 83%). A significant correlation was observed between groundspeed and altitude of the GPS data ($\rho = 0.48$, $p \ll 0.001$ by Spearman's test).

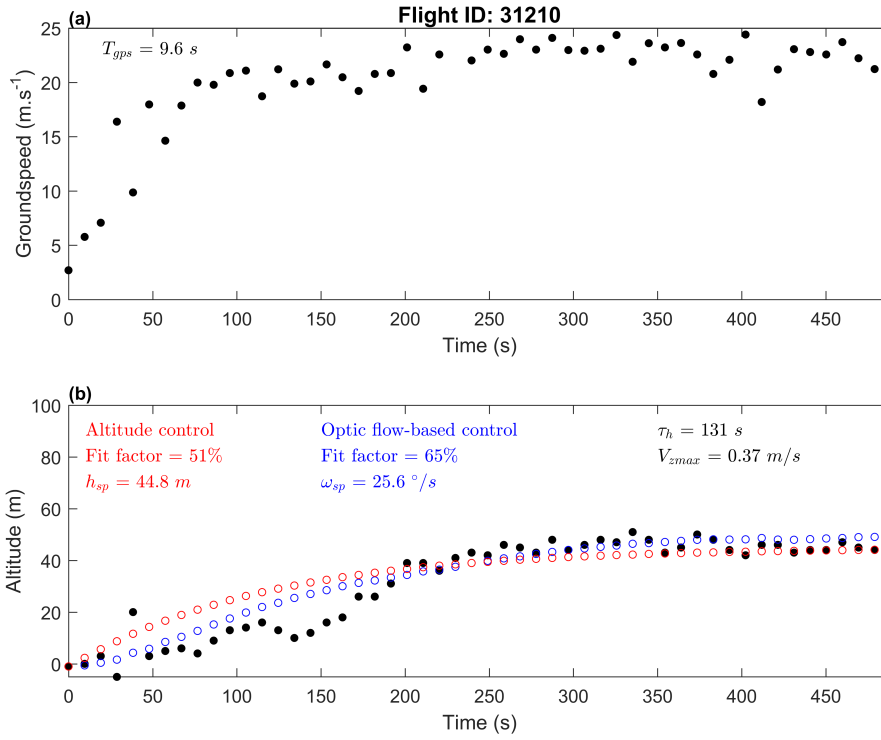


Figure S15: (a) Groundspeed of the gull ID31210 tracked with the GPS. (b) Altitude of the gull: black dots represent the GPS data, red dots represent the gull altitude on the basis of an altitude-based control model (fit factor: 51%), and the blue dots represent the gull altitude on the basis of an optic flow-based control model (fit factor: 65%). A significant correlation was observed between groundspeed and altitude of the GPS data ($\rho = 0.70$, $p \ll 0.001$ by Spearman's test).

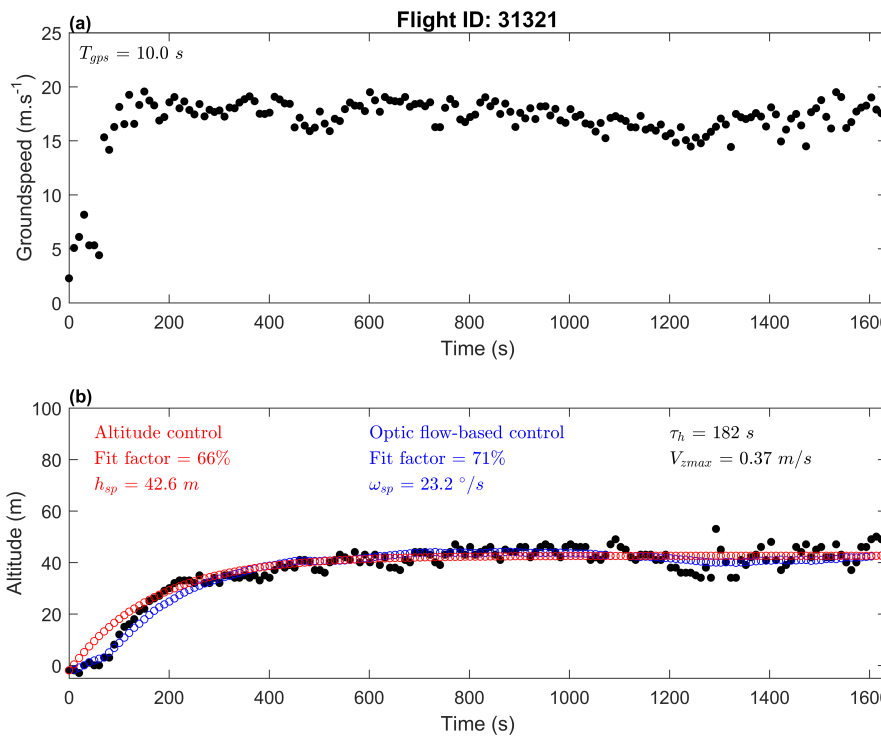


Figure S16: (a) Groundspeed of the gull ID31321 tracked with the GPS. (b) Altitude of the gull: black dots represent the GPS data, red dots represent the gull altitude on the basis of an altitude-based control model (fit factor: 66%), and the blue dots represent the gull altitude on the basis of an optic flow-based control model (fit factor: 71%). A significant correlation was observed between groundspeed and altitude of the GPS data ($\rho = 0.22$, $p \ll 0.001$ by Spearman's test).

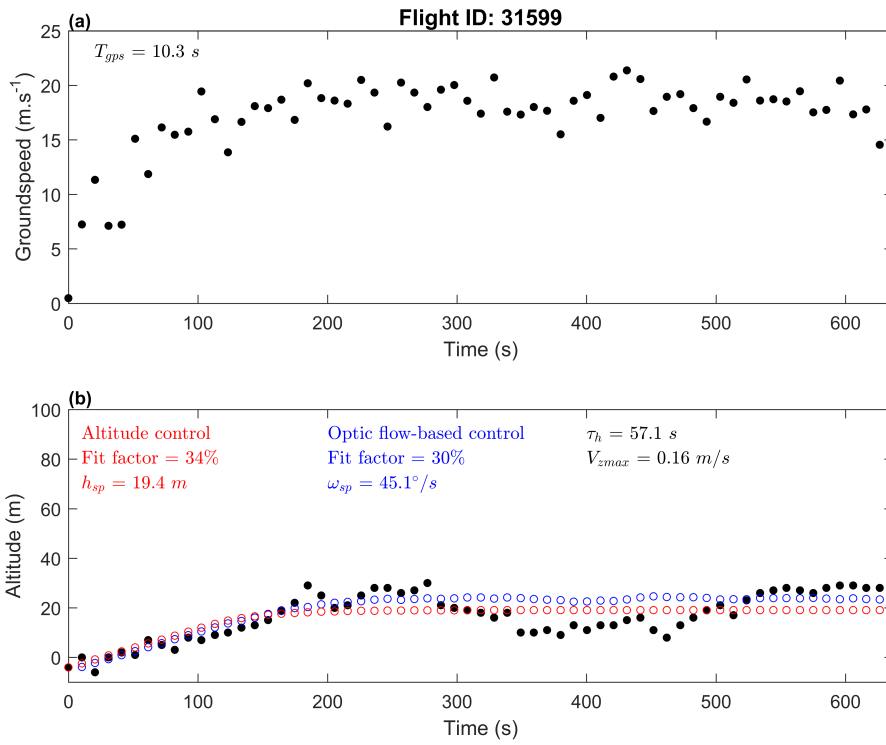


Figure S17: (a) Groundspeed of the gull ID31599 tracked with the GPS. (b) Altitude of the gull: black dots represent the GPS data, red dots represent the gull altitude on the basis of an altitude-based control model (fit factor: 34%), and the blue dots represent the gull altitude on the basis of an optic flow-based control model (fit factor: 30%). A significant correlation was observed between groundspeed and altitude of the GPS data ($\rho = 0.46$, $p \ll 0.001$ by Spearman's test).

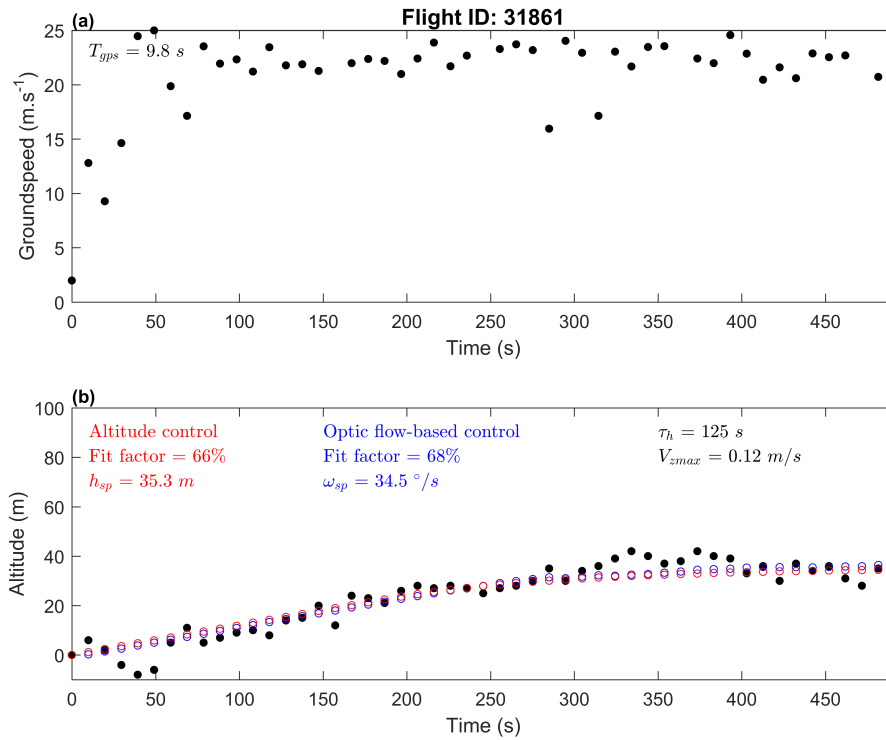


Figure S18: (a) Groundspeed of the gull ID31861 tracked with the GPS. (b) Altitude of the gull: black dots represent the GPS data, red dots represent the gull altitude on the basis of an altitude-based control model (fit factor: 66%), and the blue dots represent the gull altitude on the basis of an optic flow-based control model (fit factor: 68%). No significant correlation was observed between groundspeed and altitude of the GPS data.

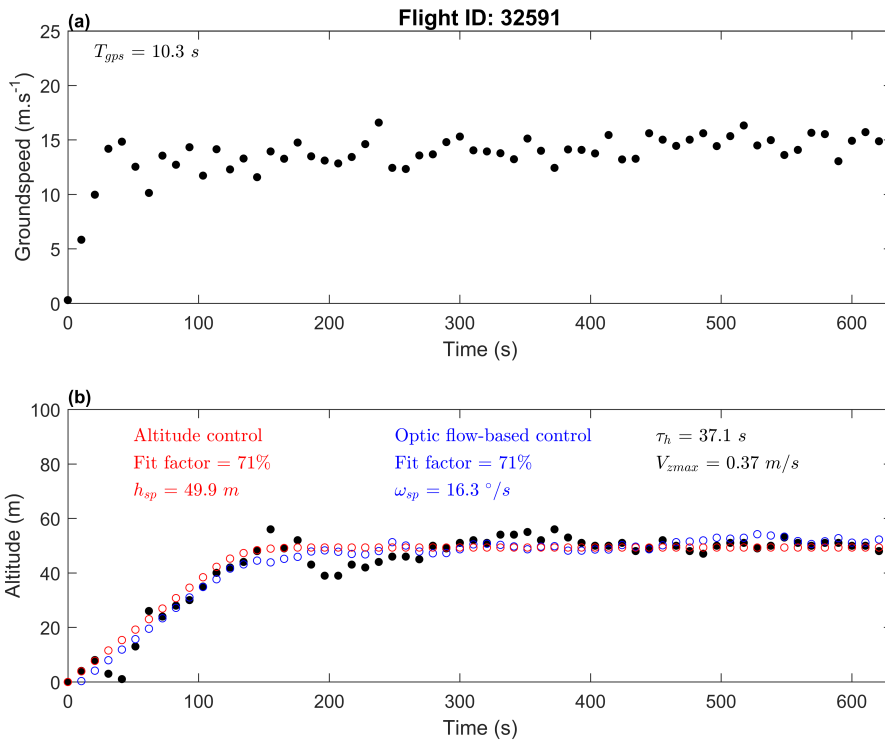


Figure S19: (a) Groundspeed of the gull ID32591 tracked with the GPS. (b) Altitude of the gull: black dots represent the GPS data, red dots represent the gull altitude on the basis of an altitude-based control model (fit factor: 71%), and the blue dots represent the gull altitude on the basis of an optic flow-based control model (fit factor: 71%). No significant correlation was observed between groundspeed and altitude of the GPS data.

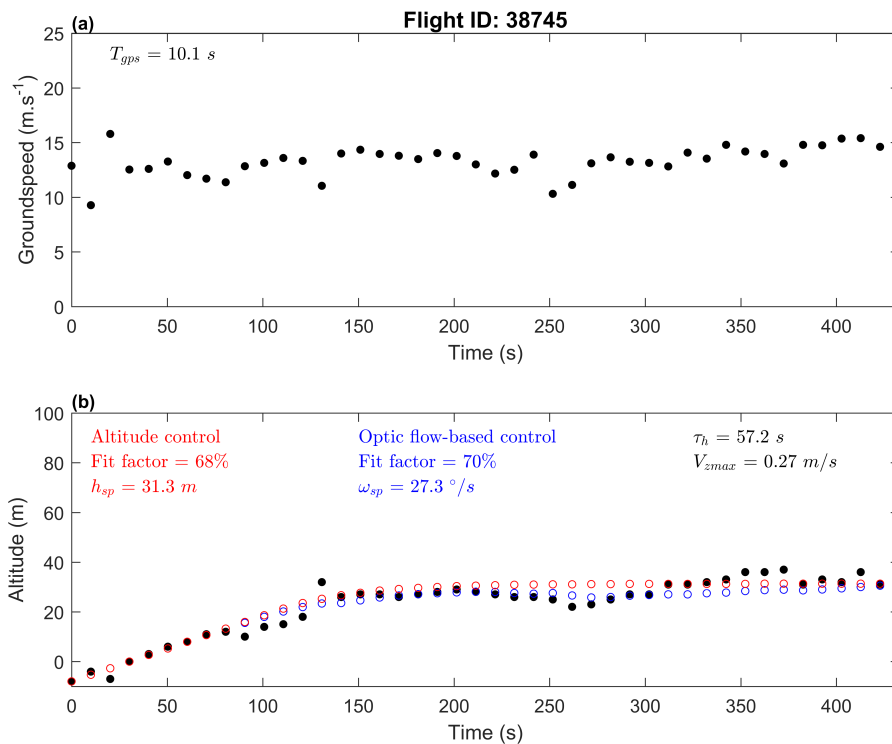


Figure S20: (a) Groundspeed of the gull ID38745 tracked with the GPS. (b) Altitude of the gull: black dots represent the GPS data, red dots represent the gull altitude on the basis of an altitude-based control model (fit factor: 68%), and the blue dots represent the gull altitude on the basis of an optic flow-based control model (fit factor: 70%). A significant correlation was observed between groundspeed and altitude of the GPS data ($\rho = 0.51$, $p \ll 0.001$ by Spearman's test).



Figure S21: Gull (*Larus fuscus*) flying above the Baltic sea. The state of the sea while gulls are flying is typically with a Beaufort number of 3 to 4. Photographic credit and courtesy from Aron Hejdström.